

# A Static Reduced-Order Multiple-Model Adaptive Estimator for Noise Identification

Joe Khalife, *Member, IEEE* and Zaher M. Kassas, *Senior Member, IEEE*

**Abstract**—A reduced-order multiple-model (MM) estimator for noise identification in dynamic stochastic systems is developed. The unknown noise statistics are assumed to be static. While a standard static MM estimator does not grow exponentially over time, its computational complexity grows exponentially with the number of modes. The proposed algorithm reduces the computational complexity of MM estimation from exponential to polynomial by constructing a significantly smaller set of mode models which are updated every time step. It is assumed that the constructed mode models do not change significantly between time steps, which in turn holds if the smoothness of the mode probabilities is guaranteed. It is shown that in the case where there is “enough” statistical distinction between the noise modes, the proposed reduced-order MM estimator converges to the standard MM estimator. The proposed reduced-order MM estimator is evaluated using Monte Carlo simulations, showing that it performs nearly similar to the standard MM estimator with a fraction of its complexity. The numerical example shows less than a 2% increase in the root mean-squared errors (RMSEs) of the reduced-order MM estimator from the standard one, while the reduction in the number of filters in the reduced-order MM estimator is 300%. To further validate the proposed filter, experimental results are presented of an unmanned aerial vehicle (UAV) navigating with terrestrial signals of opportunity. Opportunistic navigation serves a relevant application for MM-based estimation, as system parameters, namely the statistics of the clock error dynamics of opportunistic sources, are unknown and must be adaptively estimated. The experimental results show a UAV navigating for more than 5 minutes over a trajectory of more than 3 km, achieving a final position error of 6.21 m obtained using the standard MM estimator versus a final position error of 6.25 m obtained using the proposed reduced-order MM estimator. A standard extended Kalman filter (EKF) was implemented for comparative analysis, showing a final error of 40.03 m. In the experiments, the reduced-order MM estimator was implemented with 16 filters, while the standard MM was implemented with 256 filters.

**Index Terms**—Multiple-model estimation, adaptive estimation, noise identification, navigation, signals of opportunity.

## I. INTRODUCTION

The ability to adaptively estimate unknown or poorly modeled system parameters is of particular interest in the ever advancing level of autonomy of ground, aerial, and space vehicles. Consider a self-driving car or an unmanned aerial vehicle (UAV) entering a poorly modeled, dynamic stochastic environment, such as an urban intersection [1], [2] or a signal

landscape [3], [4]. As the vehicle navigates its environment, it must estimate its own states simultaneously with the environment’s states, while refining its models of the surrounding environment.

Adaptive estimation approaches [5] can be categorized into Bayesian [6]–[8], covariance matching [9]–[11], correlation [12]–[14], maximum likelihood (ML) [15]–[17], and hybrid methods. A popular Bayesian technique is the multiple-model (MM) estimator. However, such estimators suffer from the curse of dimensionality in the presence of mode-switching [18], [19]. Covariance matching techniques rely on the principle of making the time average of squared innovations consistent with the ensemble average; hence, they implicitly assume ergodicity of the noise. Tuning the process noise covariance is typically done in an ad-hoc manner, making the convergence of these techniques questionable [20], [21]. Correlation methods assume ergodicity of the noise and rely on establishing relationships between the noise statistics and the autocorrelation of the measurement or residual sequences. They have been shown to be a fruitful approach [22]–[24]. In ML techniques, the likelihood function is maximized to obtain estimates of the noise statistics, and the chain rule of probability distributions is typically invoked. A unique solution is only guaranteed whenever the dimension of the observation vector is greater than or equal to the dimension of the state vector [25], [26]. The most popular hybrid techniques are the MM adaptive estimator with mode switching [27], [28] and the interacting multiple-model (IMM) estimator [29], [30]. MM estimation has been used in a variety of applications, ranging from positioning and navigation [31], [32], target tracking [33], [34], air traffic control [35], [36], fault detection [37], [38], cognitive radio [39], [40], and many more. MM estimators have been “adapted” to estimating process and measurement noise statistics [41].

Both MM and IMM estimators maintain a bank of Kalman filters (KFs) matched to the various modes at which the system may be operating. The innovation likelihoods from each filter are used to weight the filter estimates to form a combined state estimate. The standard static MM adaptive estimator directly uses these likelihoods as adaptive weights, which could cause the filter to converge onto a particular mode. To rectify this behavior, minimum threshold probabilities are typically assigned to each filter. The IMM circumvents this problem with the introduction of an interaction/mixing step in which state estimates given to the bank of filters are calculated at each time step using the weighted estimates of the previous time step. While the IMM and its derivatives reduce the computational complexity as a function of time, the literature falls short on addressing the computational complexity of

This work was supported in part by the Air Force Office of Scientific Research (AFOSR) under Grant FA9550-22-1-0476 and in part by the National Science Foundation (NSF) under Grant 2240512.

J. Khalife was with the Department of Mechanical and Aerospace Engineering, University of California, Irvine, CA, USA. Z. Kassas is with Department of Electrical and Computer Engineering, The Ohio State University, Columbus, OH, USA. (email: khalifej@uci.edu and zkassas@ieee.org).  
Corresponding author: Z. Kassas.

MM-based estimator as a function of the number of possible modes.

This paper considers the following problem. A stochastic linear time-varying (LTV) system with  $N$  process noise elements, each of which can be in  $M$  modes. As such, a full implementation of standard MM estimators requires  $M^N$  filters to exhaust all possible modes. This exploding complexity renders MM estimators impractical for moderately large-scale systems. This paper aims to develop a reduced-order MM estimator that only requires  $M \cdot N$  filters. A particular application that would benefit from such reduction in complexity is navigation with signals of opportunity (SOPs), which are ambient signals not intended for navigation purposes [42]. SOPs have been demonstrated to be a promising complement or alternative to global navigation satellite system (GNSS) signals in GNSS-challenged environments [43], [44]. Examples of SOPs include AM/FM radio [45], [46], digital television [47], [48], cellular [49]–[52], and low Earth orbit (LEO) satellites [53]–[56]. Cellular signals proved to be particularly attractive due to their spatial and spectral diversity, high received power, and cost-free usage of their downlink synchronization signals. Cellular SOP receivers were designed to extract navigation observables from such signals [57]–[61], e.g., pseudorange and carrier phase measurements. Both the pseudorange and carrier phase measurements give a measure of the range between the transmitter and receiver up to some bias due to the difference between the transmitter’s and receiver’s clocks. The cellular SOP transmitters, known as base transceiver stations (BTSs), may be asynchronous and have unknown clock biases, which are dynamic and stochastic processes. When the statistics of these processes are unknown to the estimator, the filter will be mismatched to the true model, which in turn would degrade the estimation performance and more dangerously, could cause filter divergence altogether. One way to circumvent this mismatch is to use an adaptive MM estimator, where each estimator is matched to the statistics of some possible clock oscillator quality. A preliminary study demonstrated the efficacy of this approach, where two modes per transmitter were employed, one pertaining to a low quality oscillator and one to a high quality oscillator, and the mode probability was used as a weight [62].

The number of estimators needed for a standard MM estimator grows exponentially with the number of transmitters, especially in the case of aerial vehicle navigation, where the number of visible transmitters increases due to favorable radio propagation channels [63]. Assuming two possible models per transmitter clock, employing a standard MM estimator,  $2^8 = 1024$  filters would be needed for 8 transmitters. As the number of transmitters increases even further; which could easily happen with LEO SOPs [64], [65], where hundreds of LEO satellites could be simultaneously visible [4]; the computational complexity of MM estimators becomes practically infeasible to implement on small UAVs with limited computational power.

Motivated by the need of a computationally efficient MM estimator, the contributions of this paper are as follows:

- A reduced-order MM estimator is proposed to adaptively estimate the process and measurement noise covariance

in stochastic LTV systems. The proposed algorithm performs nearly similar to a standard MM estimator with a fraction of the computational complexity.

- A sufficient condition for the reduced-order MM estimator to converge to a standard estimator is derived.
- Monte Carlo simulations are presented to evaluate the proposed algorithm, showing a less than 2% difference in the root mean-squared error (RMSE) of the proposed algorithm compared to the standard MM estimator.
- Experimental results are presented, showing a UAV navigating for more than 5 minutes over a trajectory of more than 3 km with the proposed algorithm. The reduced-order MM estimator is compared with a standard MM estimator and a standard extended Kalman filter (EKF). A final position error of 6.21 m is obtained using the standard MM estimator implemented with 256 filters while a final position error of 6.25 m is obtained using the proposed reduced-order MM estimator implemented with 16 filters only.

The remainder of this paper is organized as follows. Section II provides the system model and gives an overview of standard MM estimation. Section III describes the reduced-order MM algorithm. Section IV presents simulation results. Section V presents experimental results. Concluding remarks are given in Section VI.

## II. SYSTEM MODEL AND MULTIPLE MODEL ESTIMATION OVERVIEW

This section presents the models adopted in the paper and gives an overview of MM estimators.

### A. System Model

Consider the following discrete-time LTV system

$$\mathbf{x}(k+1) = \mathbf{F}(k)\mathbf{x}(k) + \mathbf{w}(k) \quad (1)$$

$$\mathbf{z}(k) = \mathbf{H}(k)\mathbf{x}(k) + \mathbf{v}(k), \quad k = 0, 1, \dots, \quad (2)$$

where  $\mathbf{x}(k) \in \mathbb{R}^{n_x}$  is the state vector;  $\mathbf{F}(k)$  is the state transition matrix;  $\mathbf{z}(k) \in \mathbb{R}^{n_z}$  is the measurement vector;  $\mathbf{H}(k)$  is the output matrix; and  $\mathbf{w}(k)$  and  $\mathbf{v}(k)$  are zero-mean white Gaussian random sequences with covariances  $\mathbf{Q}(k)$  and  $\mathbf{R}(k)$ , respectively. Let  $Z^k$  denote the set of all measurements up to time  $k$ , i.e.,  $Z^k \triangleq \{\mathbf{z}(\kappa)\}_{\kappa=0}^k$ . The time index  $k$  will be subsequently dropped for compactness of notation, unless explicitly specified. Consider the process noise vector  $\mathbf{w} = [w_1, w_2, \dots, w_{n_x}]^\top$ . Each  $w_l$  can be in one of  $r_l$  modes, where each particular mode has a corresponding variance  $\sigma_l^2$  and cross-covariance  $\sigma_{ll'}$  for  $l' \in \{1, \dots, n_x\} \setminus l$ . Let  $L$  denote the total number of process noise elements for which  $r_l > 1$ . The resulting process noise covariance can always be expressed as a linear combination of these  $L$  elements as given by

$$\mathbf{Q} = \sum_{l=1}^L \mathbf{\Gamma}_l \mathbf{Q}^l \mathbf{\Gamma}_l^\top, \quad (3)$$

where  $\mathbf{\Gamma}_l$  are known constant matrices and  $\mathbf{Q}^l \in \{\mathbf{Q}_i^l\}_{i=1}^{r_l}$ , and  $r_l$  is number of possible “modes” of process noise element  $l$ . In

this paper, it is assumed that all elements of the process noise covariance matrix are in a fixed but unknown mode  $\forall k \geq 0$ , i.e.,

$$\mathbf{Q}^l = \mathbf{Q}_{n_l}^l, \quad \forall k \geq 0, \quad (4)$$

where  $n_l$  is the active mode of the  $l$ th element. To illustrate (3) and (4), consider a double integrator system driven by process noise. This system is typically used to model the behavior of crystal oscillator clocks, a crucial element in radionavigation. The discrete-time process noise covariance of these models is expressed as

$$\mathbf{Q} = \begin{bmatrix} S_1 T + S_2 \frac{T^3}{3} & S_2 \frac{T^2}{2} \\ S_2 \frac{T^2}{2} & S_2 T \end{bmatrix}, \quad (5)$$

where  $T$  is the sampling time and  $S_1$  and  $S_2$  are the continuous-time power spectra of the clock bias and drift. The quantities  $S_1$  and  $S_2$  vary with the quality of the oscillator. When these quantities are unknown, one can use an MM estimator to estimate them along with the clock states. It is assumed that  $S_1$  and  $S_2$  are given from the sets  $\mathcal{S}_1$  and  $\mathcal{S}_2$ , respectively. A standard MM estimator would require a number of filters that is equal to the product of the cardinalities of  $\mathcal{S}_1$  and  $\mathcal{S}_2$ . The goal of the reduced-order MM is to adaptively estimate  $S_1$  and  $S_2$  with lower complexity. As such, one can re-write the process noise covariance in (5) as

$$\mathbf{Q} = \sum_{l=1}^2 \mathbf{\Gamma}_l \mathbf{Q}^l \mathbf{\Gamma}_l^T, \quad (6)$$

where

$$\mathbf{Q}^1 = S_1 T, \quad \mathbf{Q}^2 = \begin{bmatrix} S_2 \frac{T^3}{3} & S_2 \frac{T^2}{2} \\ S_2 \frac{T^2}{2} & S_2 T \end{bmatrix}, \quad \mathbf{\Gamma}_1 = [1, 0]^T, \quad \mathbf{\Gamma}_2 = \mathbf{I}_{2 \times 2}, \quad (7)$$

and  $\mathbf{I}_{n \times n}$  is the  $n \times n$  identity matrix. Note that  $\mathbf{\Gamma}_1$  and  $\mathbf{\Gamma}_2$  are constant and known matrices. The quantity  $\mathbf{Q}^1$  is solely dependent on  $S_1$ , which is unknown but is given from the set  $\mathcal{S}_1$  and  $\mathbf{Q}^2$  is solely dependent on  $S_2$ , which is also unknown but is given from the set  $\mathcal{S}_2$ . As will be shown in the next Section, expressing  $\mathbf{Q}$  as in (3) will be crucial in the formulation of the reduced-order MM estimator, as it allows to estimate the process noise covariance of each element separately from the rest, reducing the number of filters needed to the sum of cardinalities of  $\mathcal{S}_1$  and  $\mathcal{S}_2$  instead of their product.

Similarly to the process noise covariance, the measurement noise covariance can generally be expressed as a linear combination of  $J$  elements as given by

$$\mathbf{R} = \sum_{j=1}^J \mathbf{\Psi}_j \mathbf{R}^j \mathbf{\Psi}_j^T, \quad (8)$$

where  $\mathbf{\Psi}_j$  are known constant matrices and  $\mathbf{R}^j \in \left\{ \mathbf{R}_i^j \right\}_{i=1}^{s_j}$ , and  $s_j$  is number of possible modes of measurement noise element  $j$ . Moreover, it is assumed that all elements of the measurement noise covariance matrix are in a fixed but unknown mode  $\forall k \geq 0$ , i.e.,

$$\mathbf{R}^j = \mathbf{R}_{o_j}^j, \quad \forall k \geq 0, \quad (9)$$

where  $o_j$  is the active mode of the  $j$ th element. Note that it is assumed that  $\mathbf{Q} \succ 0$  and  $\mathbf{R} \succ 0$ .

## B. Overview of the Standard Multiple Model Estimator

In MM estimation, the system is assumed to obey one of a finite number of modes, and a bank of estimators (usually KFs) run in parallel, where each filter is matched to a particular mode. A state estimate is computed by summing the individual filter estimates, weighted by their respective innovation likelihoods [66].

1) *Simple MM Estimator Formulation:* A single cycle of the standard MM estimator for  $r = 2$  models is depicted in Fig. 1, with the following notational definitions:

$r$	Number of filters
$i$	$\{1, \dots, r\} \in \mathbb{N}$
$M_i$	Hypothesis that mode $i$ is active
$\hat{\mathbf{x}}^i(k k)$	State estimate of filter $i$
$\mathbf{P}^i(k k)$	Estimation error covariance of filter $i$
$\Lambda_i(k+1)$	Innovation likelihood of filter $i$
$\hat{\mathbf{x}}^i(k+1 k+1)$	Updated state estimate of filter $i$
$\mathbf{P}^i(k+1 k+1)$	Updated estimation error covariance of filter $i$
$\mu_i(k+1)$	Mode probability of filter $i$
$\hat{\mathbf{x}}_{\text{MM}}(k+1 k+1)$	Combined state estimate in the MM estimator
$\mathbf{P}_{\text{MM}}(k+1 k+1)$	Combined estimation error covariance in the MM estimator

The MM estimator consists of three stages: filtering, mode probability update, and combination, which are summarized next.

- 1) **Mode-Matched Filtering:** This stage performs a regular KF update (prediction and correction), for each KF in the bank, where each filter is matched to a particular mode to produce estimates  $\hat{\mathbf{x}}^i(k+1|k+1)$  and associated estimation error covariance  $\mathbf{P}^i(k+1|k+1)$ . It also calculates the innovation likelihood functions according to

$$\Lambda_i(k+1) = \mathcal{N}[\mathbf{v}^i(k+1); \mathbf{0}, \mathbf{S}^i(k+1)], \quad (10)$$

where  $\mathcal{N}[\mathbf{x}; \boldsymbol{\mu}, \boldsymbol{\Sigma}]$  denotes the multivariate Gaussian probability density function (pdf) with mean vector  $\boldsymbol{\mu}$  and covariance matrix  $\boldsymbol{\Sigma}$  evaluated at some vector  $\mathbf{x}$ ,  $\mathbf{v}^i(k+1)$  is the innovation vector in filter  $i$ , and  $\mathbf{S}^i(k+1)$  is the innovation covariance in filter  $i$ .

- 2) **Mode probability update:** This stage updates the mode probabilities based on the innovation likelihoods using Bayes' formula, which can be shown to be

$$\mu_i(k+1) = \frac{\Lambda_i(k+1)\mu_i(k)}{\sum_{j=1}^r \Lambda_j(k+1)\mu_j(k)}. \quad (11)$$

- 3) **State estimate and covariance combination:** This stage combines the state estimates and estimation error covariances from the individual filters by weighting  $\hat{\mathbf{x}}^i(k+1|k+1)$

$1|k+1)$  and  $\mathbf{P}^i(k+1|k+1)$  by their respective mode probabilities  $\mu_i(k+1)$  according to

$$\hat{\mathbf{x}}_{\text{MM}}(k+1|k+1) = \sum_{j=1}^r \mu_j(k+1) \hat{\mathbf{x}}^j(k+1|k+1), \quad (12)$$

$$\begin{aligned} \mathbf{P}_{\text{MM}}(k+1|k+1) = & \sum_{j=1}^r \mu_j(k+1) \left\{ \mathbf{P}^j(k+1|k+1) \right. \\ & + \left[ \hat{\mathbf{x}}^j(k+1|k+1) - \hat{\mathbf{x}}_{\text{MM}}(k+1|k+1) \right] \\ & \cdot \left[ \hat{\mathbf{x}}^j(k+1|k+1) - \hat{\mathbf{x}}_{\text{MM}}(k+1|k+1) \right]^T \left. \right\}. \end{aligned} \quad (13)$$

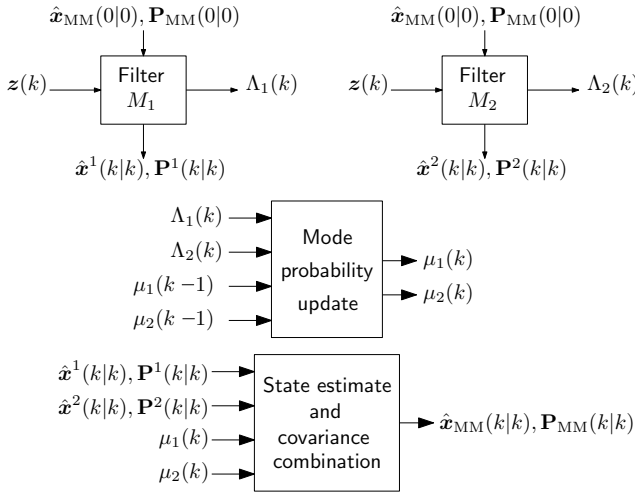


Fig. 1. Standard MM estimator for  $r = 2$  fixed models.

After some time, the mode probability of the active mode in the MM estimator will converge to unity and the others to zero. After convergence, the estimate and estimation error covariance will converge to those of a KF matched to the true active mode. Let  $\hat{\mathbf{x}}(k|k)$  and  $\mathbf{P}(k|k)$  denote the matched estimate and estimation error covariance. As such, after convergence, the following holds:  $\hat{\mathbf{x}}_{\text{MM}}(k|k) = \hat{\mathbf{x}}(k|k)$  and  $\mathbf{P}_{\text{MM}}(k|k) = \mathbf{P}(k|k)$ .

2) *MM Estimator Formulation for the System in (1)–(2):* Let  $M_{i_l}^l$  denote the event that the  $i_l$ th mode of the  $l$ th process noise element is active and  $N_{t_j}^j$  the fact that the  $t_j$ th mode of the  $j$ th measurement noise element is active. Next, let  $\mu_{i_1, \dots, i_L, t_1, \dots, t_J}(k)$  denote the probability that  $\{M_{i_1}^1, \dots, M_{i_L}^L, N_{t_1}^1, \dots, N_{t_J}^J\}$  are active given  $Z^k$ , hence

$$\mu_{i_1, \dots, i_L, t_1, \dots, t_J}(k) = \Pr [M_{i_1}^1, \dots, M_{i_L}^L, N_{t_1}^1, \dots, N_{t_J}^J | Z^k]. \quad (14)$$

In the standard MM approach, it is assumed that there is a filter matched for each combination  $\{M_{i_1}^1, \dots, M_{i_L}^L, N_{t_1}^1, \dots, N_{t_J}^J\}$ . Let  $\hat{\mathbf{x}}_{i_1, \dots, i_L, t_1, \dots, t_J}(k|k)$  denote the current estimate in the filter matched to  $\{M_{i_1}^1, \dots, M_{i_L}^L, N_{t_1}^1, \dots, N_{t_J}^J\}$  and  $\mathbf{P}_{i_1, \dots, i_L, t_1, \dots, t_J}(k|k)$  its corresponding estimation error covariance. Similarly to (12), the combined estimate in this case will be given by

$$\begin{aligned} \hat{\mathbf{x}}_{\text{MM}}(k|k) = & \sum_{i_1} \dots \sum_{i_L} \sum_{t_1} \dots \sum_{t_J} \mu_{i_1, \dots, i_L, t_1, \dots, t_J}(k) \\ & \cdot \hat{\mathbf{x}}_{i_1, \dots, i_L, t_1, \dots, t_J}(k|k), \end{aligned} \quad (15)$$

with the estimation error covariance

$$\begin{aligned} \mathbf{P}_{\text{MM}}(k|k) = & \sum_{i_1} \dots \sum_{i_L} \sum_{t_1} \dots \sum_{t_J} \mu_{i_1, \dots, i_L, t_1, \dots, t_J}(k) \\ & \cdot \left\{ \mathbf{P}_{i_1, \dots, i_L, t_1, \dots, t_J}(k|k) \right. \\ & + \left[ \hat{\mathbf{x}}_{i_1, \dots, i_L, t_1, \dots, t_J}(k|k) - \hat{\mathbf{x}}_{\text{MM}}(k|k) \right] \\ & \cdot \left[ \hat{\mathbf{x}}_{i_1, \dots, i_L, t_1, \dots, t_J}(k|k) - \hat{\mathbf{x}}_{\text{MM}}(k|k) \right]^T \left. \right\}. \end{aligned} \quad (16)$$

Consequently, in order to run an MM estimator for the system defined in (1)–(2), the number of filters needed is given by

$$N_{\text{filters}} = \prod_{l=1}^L r_l \prod_{j=1}^J s_j. \quad (17)$$

Assuming  $r_1 = r_2 = \dots = r_L = r$  and  $s_1 = s_2 = \dots = s_J = s$ , then  $N_{\text{filters}} = r^L s^J$ , which grows exponentially with the number of elements  $L$  and  $J$ . The next section proposes a near-optimal MM-based estimator where the number of required filters does not scale exponentially.

### III. REDUCED-ORDER MM ESTIMATOR

The reduced-order MM estimator is developed next.

#### A. Motivation of the Reduced-Order MM Estimator

MM estimators were also used to estimate the unknown process noise statistics in [67], where a bank of two KFs are identically initialized with the exception of  $\mathbf{Q}^i$ . One of the filters was initialized with an upper-bound  $\mathbf{Q}_{\text{max}}$ , while the other is initialized with a lower-bound  $\mathbf{Q}_{\text{min}}$ , corresponding to the worst and best case process noise scenarios. In this scheme, the noise covariance estimate  $\hat{\mathbf{Q}}$  is computed as

$$\hat{\mathbf{Q}}(k) = \sum_{i=1}^2 \mu_i(k) \mathbf{Q}^i(k). \quad (18)$$

This can be similarly done for the measurement covariance as

$$\hat{\mathbf{R}}(k) = \sum_{i=1}^2 \mu_i(k) \mathbf{R}^i(k). \quad (19)$$

This can be generalized for the case of a MM estimator for system (1)–(2), where

$$\begin{aligned} \hat{\mathbf{Q}}(k) = & \sum_{i_1} \dots \sum_{i_L} \sum_{t_1} \dots \sum_{t_J} \mu_{i_1, \dots, i_L, t_1, \dots, t_J}(k) \sum_{l=1}^L \Gamma_l \mathbf{Q}_{i_l}^l \Gamma_l^T \\ = & \sum_{l=1}^L \sum_{i_1} \dots \sum_{i_L} \Gamma_l \mathbf{Q}_{i_l}^l \Gamma_l^T \sum_{t_1} \dots \sum_{t_J} \mu_{i_1, \dots, i_L, t_1, \dots, t_J}(k), \end{aligned} \quad (20)$$

and

$$\begin{aligned} \hat{\mathbf{R}}(k) = & \sum_{i_1} \dots \sum_{i_L} \sum_{t_1} \dots \sum_{t_J} \mu_{i_1, \dots, i_L, t_1, \dots, t_J}(k) \sum_{j=1}^J \Psi_j \mathbf{R}_{t_j}^j \Psi_j^T \\ = & \sum_{j=1}^J \sum_{t_1} \dots \sum_{t_J} \Psi_l \mathbf{R}_{t_j}^j \Psi_j^T \sum_{i_1} \dots \sum_{i_L} \mu_{i_1, \dots, i_L, t_1, \dots, t_J}(k). \end{aligned} \quad (21)$$

The following lemma motivates the main idea behind the reduced-order MM estimator.

**Lemma III.1.** *Consider a MM estimator for the system in (1)–(2). Then, the process noise and measurement noise covariance estimates may be expressed as*

$$\hat{\mathbf{Q}}(k) = \frac{1}{L} \sum_{l=1}^L \sum_{i_l} \mu_{i_l}^{q,l}(k) \bar{\mathbf{Q}}_{i_l}^l(k), \quad (22)$$

$$\hat{\mathbf{R}}(k) = \frac{1}{J} \sum_{j=1}^J \sum_{t_j} \mu_{t_j}^{r,j}(k) \bar{\mathbf{R}}_{t_j}^j(k), \quad (23)$$

where  $\mu_{i_l}^{q,l}(k)$  and  $\mu_{t_j}^{r,j}(k)$  are some appropriately defined probabilities, i.e.,  $\sum \mu_{i_l}^{q,l}(k) = 1$  and  $\sum \mu_{t_j}^{r,j}(k) = 1$ , and

$$\bar{\mathbf{Q}}_{i_m}^m(k) \triangleq \mathbf{\Gamma}_m \mathbf{Q}_{i_m}^m \mathbf{\Gamma}_m^T + \bar{\mathbf{Q}}^m(k), \quad (24)$$

$$\bar{\mathbf{R}}_{i_p}^p(k) \triangleq \mathbf{\Psi}_p \mathbf{R}_{i_p}^p \mathbf{\Psi}_p^T + \bar{\mathbf{R}}^p(k), \quad (25)$$

where

$$\bar{\mathbf{Q}}^m(k) \triangleq \sum_{\substack{l=1 \\ l \neq m}}^L \sum_{i_l} \mu_{i_l}^{q,l}(k) \mathbf{\Gamma}_l \mathbf{Q}_{i_l}^l \mathbf{\Gamma}_l^T, \quad (26)$$

$$\bar{\mathbf{R}}^p(k) \triangleq \sum_{\substack{j=1 \\ j \neq p}}^J \sum_{t_j} \mu_{t_j}^{r,j}(k) \mathbf{\Psi}_j \mathbf{R}_{t_j}^j \mathbf{\Psi}_j^T. \quad (27)$$

**Proof.** See Appendix .

Lemma III.1 implies that the estimated process and measurement noise covariances can be expressed as a sum of  $\sum_{l=1}^L r_l$  and  $\sum_{j=1}^J s_j$  terms, respectively. For simplicity, assume  $J = 1$  with  $s_1 = s = 1$  and  $r_l = r$ . Then, (22) can be interpreted as the estimated process noise covariance from  $L$  banks of filters, each bank with  $r$  sub-banks of filters, with each particular filter matched to the process noise covariance given in (24). A similar interpretation can be made for  $\hat{\mathbf{R}}(k)$  in the general case. Consequently, when all  $L$  and  $J$  banks of filters converge, i.e., the mode probabilities  $\mu_{i_l}^{q,l}(k)$  and  $\mu_{t_j}^{r,j}(k)$  become

$$\mu_{i_l}^{q,l}(k) = \mu_{i_l}^{q,l} = \begin{cases} 1, & \text{if } i_l = n_l, \\ 0, & \text{otherwise} \end{cases}, \forall l = 1, \dots, L,$$

and

$$\mu_{t_j}^{r,j}(k) = \mu_{t_j}^{r,j} = \begin{cases} 1, & \text{if } t_j = o_j, \\ 0, & \text{otherwise} \end{cases}, \forall j = 1, \dots, J,$$

then it can be readily shown that  $\bar{\mathbf{Q}}_{i_m}^m(k) = \mathbf{Q}(k)$  and  $\bar{\mathbf{R}}_{i_p}^p(k) = \mathbf{R}(k)$ , which in turn implies that  $\hat{\mathbf{Q}}(k) = \mathbf{Q}(k)$  and  $\hat{\mathbf{R}}(k) = \mathbf{R}(k)$ .

### B. Reduced-Order MM Algorithm

Motivated by the results of Lemma III.1, the reduced-order MM estimator algorithm is developed. The proposed algorithm requires a total of  $U = \sum_{l=1}^L r_l + \sum_{j=1}^J s_j$  filters and operates similarly to the standard MM estimator with some differences highlighted in the following steps. Let  $\hat{\mu}_{i_l}^{q,l}$  denote the mode probability of the filter matched to the  $i_l$ th mode of the  $l$ th

process noise element and  $\hat{\mu}_{t_j}^{r,j}$  denote the mode probability of the filter matched to the  $t_j$ th mode of the  $j$ th measurement noise element.

1) *Model Construction:* In this stage, a model for each mode-matched filter is constructed as follows. Let  $u \in \{1, 2, \dots, U\}$  denote the  $u$ th mode-matched filter. Note that if  $u \leq \sum_{l=1}^L r_l$ , then  $u$  can be mapped to an element  $m$  of the process noise. In this case, the  $u$ th process noise covariance, which is the one matched to the  $i_m$ th mode of the  $m$ th process noise element, is constructed as

$$\hat{\mathbf{Q}}^u(k) = \mathbf{\Gamma}_m \mathbf{Q}_{i_m}^m \mathbf{\Gamma}_m^T + \hat{\mathbf{Q}}^m(k), \quad (28)$$

where

$$\hat{\mathbf{Q}}^m(k) = \sum_{\substack{l=1 \\ l \neq m}}^L \sum_{i_l} \hat{\mu}_{i_l}^{q,l}(k) \mathbf{\Gamma}_l \mathbf{Q}_{i_l}^l \mathbf{\Gamma}_l^T, \quad (29)$$

The mode-matched measurement noise covariance will be given by

$$\hat{\mathbf{R}}^u(k) = \sum_{j=1}^J \sum_{t_j} \hat{\mu}_{t_j}^{r,j}(k) \mathbf{\Psi}_j \mathbf{R}_{t_j}^j \mathbf{\Psi}_j^T. \quad (30)$$

Alternatively, if  $u > \sum_{l=1}^L r_l$  then  $u$  can be mapped to the  $t_m$ th model of the  $m$ th measurement noise element. In this case, the mode-matched process noise covariance is constructed as

$$\hat{\mathbf{Q}}^u(k) = \sum_{l=1}^L \sum_{i_l} \hat{\mu}_{i_l}^{q,l}(k) \mathbf{\Gamma}_l \mathbf{Q}_{i_l}^l \mathbf{\Gamma}_l^T. \quad (31)$$

The mode-matched measurement noise covariance will be given by

$$\hat{\mathbf{R}}^u(k) = \mathbf{\Psi}_m \mathbf{R}_{t_m}^m \mathbf{\Psi}_m^T + \hat{\mathbf{R}}^m(k), \quad (32)$$

where

$$\hat{\mathbf{R}}^m(k) = \sum_{\substack{j=1 \\ j \neq m}}^J \sum_{t_j} \hat{\mu}_{t_j}^{r,j}(k) \mathbf{\Psi}_j \mathbf{R}_{t_j}^j \mathbf{\Psi}_j^T. \quad (33)$$

2) *Mode-Matched Filtering:* After model construction, each filter is updated and the likelihood functions denoted by  $\Lambda_{i_l}^l(k)$  and  $\Lambda_{t_j}^j(k)$  are computed similarly to the MM estimator shown in (10). For details about mode-matched filtering and likelihood function calculations, the reader is referred to [66].

3) *Mode probability Update:* Similar to the standard MM equations, the mode probabilities  $\hat{\mu}_{i_l}^{q,l}$  and  $\hat{\mu}_{t_j}^{r,j}$  are updated using  $\Lambda_{i_l}^l(k)$  and  $\Lambda_{t_j}^j(k)$  according to (11). This step assumes that the constructed models do not vary significantly between time steps. The assumption is discussed further in Subsection III-D.

4) *State Estimate and Covariance Combination:* Let  $\hat{\mathbf{x}}'_{\text{MM}}(k|k)$  and  $\mathbf{P}'_{\text{MM}}(k|k)$  denote the state estimate and covariance of the reduced-order MM estimator. Moreover, let  $\hat{\mathbf{x}}_{i_l}^{q,l}(k|k)$  and  $\mathbf{P}_{i_l}^{q,l}(k|k)$  denote the estimate and estimation error covariance maintained in the filter matched to the  $i_l$ th mode of the  $l$ th process noise element, and  $\hat{\mathbf{x}}_{t_j}^{r,j}(k|k)$  and  $\mathbf{P}_{t_j}^{r,j}(k|k)$  denote the estimate and estimation error covariance maintained in the filter matched to the  $t_j$ th mode of the  $j$ th

measurement noise element. Subsequently, the state estimate and covariance combination is performed similarly to the standard MM estimator and is given by

$$\hat{\mathbf{x}}'_{\text{MM}}(k|k) = \frac{1}{L+J} \left[ \sum_{l=1}^L \sum_{i_l} \hat{\mu}_{i_l}^{q,l}(k) \hat{\mathbf{x}}_{i_l}^{q,l}(k|k) + \sum_{j=1}^J \sum_{t_j} \hat{\mu}_{t_j}^{r,j}(k) \hat{\mathbf{x}}_{t_j}^{r,j}(k|k) \right]. \quad (34)$$

The estimation error covariance is given by

$$\begin{aligned} \hat{\mathbf{P}}'_{\text{MM}}(k|k) = \frac{1}{L+J} & \left\{ \sum_{l=1}^L \sum_{i_l} \hat{\mu}_{i_l}^{q,l}(k) \left\{ \mathbf{P}_{i_l}^{q,l}(k|k) \right. \right. \\ & + \left[ \hat{\mathbf{x}}_{i_l}^{q,l}(k|k) - \hat{\mathbf{x}}'_{\text{MM}}(k|k) \right] \\ & \cdot \left. \left. \left[ \hat{\mathbf{x}}_{i_l}^{q,l}(k|k) - \hat{\mathbf{x}}'_{\text{MM}}(k|k) \right]^T \right\} \right. \\ & + \sum_{j=1}^J \sum_{t_j} \hat{\mu}_{t_j}^{r,j}(k) \left\{ \mathbf{P}_{t_j}^{r,j}(k|k) \right. \\ & + \left[ \hat{\mathbf{x}}_{t_j}^{r,j}(k|k) - \hat{\mathbf{x}}'_{\text{MM}}(k|k) \right] \\ & \cdot \left. \left. \left[ \hat{\mathbf{x}}_{t_j}^{r,j}(k|k) - \hat{\mathbf{x}}'_{\text{MM}}(k|k) \right]^T \right\} \right\}. \quad (35) \end{aligned}$$

Note that similar to the standard MM estimator, the process noise and measurement noise covariances may be estimated as

$$\hat{\mathbf{Q}}(k) = \sum_{l=1}^L \sum_{i_l} \hat{\mu}_{i_l}^l(k) \mathbf{\Gamma}_l \mathbf{Q}_{i_l}^l \mathbf{\Gamma}_l^T, \quad (36)$$

$$\hat{\mathbf{R}}(k) = \sum_{j=1}^J \sum_{t_j} \hat{\mu}_{t_j}^j(k) \mathbf{\Psi}_j \mathbf{R}_{t_j}^j \mathbf{\Psi}_j^T. \quad (37)$$

### C. Optimality of the Reduced-Order MM Estimator

The reduced-order MM estimator comprises  $L + J$  banks of filters, one for each process noise and measurement noise element. The  $l$ th bank of process noise elements contains a sub-bank of  $r_l$  filters, each matched to one of the  $r_l$  modes that the  $l$ th process noise element can be in. In other words, the  $l$ th bank is running  $r_l$  filters, each filter matched to a process noise covariance from the set  $\{\hat{\mathbf{Q}}_{i_l}^l(k)\}_{i_l=1}^{r_l}$ . Similarly, the  $j$ th bank of measurement noise elements contains a sub-bank of  $s_j$  filters, each matched to one of the  $s_j$  modes that the  $j$ th measurement noise element can be in. In other words, the  $j$ th bank is running  $s_j$  filters, each filter matched to a measurement noise covariance from the set  $\{\hat{\mathbf{R}}_{t_j}^j(k)\}_{t_j=1}^{s_j}$ . Recall that  $\hat{\mathbf{x}}(k|k)$  and  $\mathbf{P}(k|k)$  denote the estimate of  $\mathbf{x}$  and its associated estimation error covariance in a KF matched to the true statistics  $\mathbf{Q}$  and  $\mathbf{R}$ . As such, if the mode probabilities in the reduced-order MM converge to the right values, i.e.,

$$\hat{\mu}_{i_l}^{q,l}(k) = \hat{\mu}_{i_l}^{q,l} = \begin{cases} 1, & \text{if } i_l = n_l, \\ 0, & \text{otherwise} \end{cases}, \forall l = 1, \dots, L, \quad (38)$$

$$\hat{\mu}_{t_j}^{r,j}(k) = \hat{\mu}_{t_j}^{r,j} = \begin{cases} 1, & \text{if } t_j = o_j, \\ 0, & \text{otherwise} \end{cases}, \forall j = 1, \dots, J, \quad (39)$$

then, it can be readily shown combining (36)–(39) that the estimated process and measurement noise covariances converge to the true ones, i.e.,

$$\hat{\mathbf{Q}}(k) \rightarrow \mathbf{Q}(k), \quad \hat{\mathbf{R}}(k) \rightarrow \mathbf{R}(k). \quad (40)$$

As a result, the filters for which  $\hat{\mu}_{i_l}^{q,l} = 1$  and  $\hat{\mu}_{t_j}^{r,j} = 1$  will be matched to  $\mathbf{Q}$  and  $\mathbf{R}$ , which in turn means that their state estimate and estimation error covariances will converge to  $\hat{\mathbf{x}}(k|k)$  and  $\mathbf{P}(k|k)$ . As such, if (38) and (39) hold, then it follows that

$$\hat{\mathbf{x}}'_{\text{MM}}(k|k) \rightarrow \hat{\mathbf{x}}(k|k), \quad \hat{\mathbf{P}}'_{\text{MM}}(k|k) \rightarrow \hat{\mathbf{P}}(k|k). \quad (41)$$

In other words, if (38) and (39) hold, then the reduced-order MM estimator converges to that of a matched KF, which is known to be the optimal estimator of  $\mathbf{x}$ .

### D. Condition for Convergence

Recall that the reduced-order MM estimator employs a total of  $U = \sum_{l=1}^L r_l + \sum_{j=1}^J s_j$  filters, and that the  $u$ th mode-matched filter, where  $u \in \{1, 2, \dots, U\}$  can be mapped to an element  $m$  of the process or measurement noise. As such, let  $\hat{\mu}_{\zeta_m}^{\beta,m}(k)$  denote the estimated mode probability in the reduced-order MM estimator, which maps to  $\hat{\mu}_{i_m}^{q,m}(k)$  if  $u \leq \sum_{l=1}^L r_l$ , or to  $\hat{\mu}_{t_m}^{r,m}(k)$  otherwise. Moreover, let  $\hat{M}_{\zeta_m}^{\beta,m}(k)$  denote the process and measurement noise model assumed by the  $u$ th mode-matched filter, which can be obtained from (28)–(32). Using Bayes' formula, one can write  $\hat{\mu}_{\zeta_m}^{\beta,m}(k)$  as

$$\begin{aligned} \hat{\mu}_{\zeta_m}^{\beta,m}(k) &= \Pr \left[ \hat{M}_{\zeta_m}^{\beta,m}(k) \mid \mathbf{z}(k), Z^{k-1} \right] \\ &= \frac{\Pr \left[ \hat{M}_{\zeta_m}^{\beta,m}(k), \mathbf{z}(k) \mid Z^{k-1} \right]}{\Pr \left[ \mathbf{z}(k) \mid Z^{k-1} \right]} \\ &= \frac{\Pr \left[ \mathbf{z}(k) \mid \hat{M}_{\zeta_m}^{\beta,m}(k), Z^{k-1} \right] \Pr \left[ \hat{M}_{\zeta_m}^{\beta,m}(k) \mid Z^{k-1} \right]}{\sum_{\zeta_n} \Pr \left[ \mathbf{z}(k) \mid \hat{M}_{\zeta_n}^{\beta,m}(k), Z^{k-1} \right] \Pr \left[ \hat{M}_{\zeta_n}^{\beta,m}(k) \mid Z^{k-1} \right]}. \quad (42) \end{aligned}$$

Note that  $\Pr \left[ \hat{M}_{\zeta_m}^{\beta,m}(k) \mid Z^{k-1} \right]$  is not known but if the model estimate does not vary significantly between time steps, it can be approximated with

$$\begin{aligned} \Pr \left[ \hat{M}_{\zeta_m}^{\beta,m}(k) \mid Z^{k-1} \right] &\approx \Pr \left[ \hat{M}_{\zeta_m}^{\beta,m}(k-1) \mid Z^{k-1} \right] \\ &= \hat{\mu}_{\zeta_m}^{\beta,m}(k-1), \quad (43) \end{aligned}$$

hence the following recursion is obtained

$$\hat{\mu}_{\zeta_m}^{\beta,m}(k) \approx \alpha_{\zeta_m}^{\beta,m}(k) \cdot \hat{\mu}_{\zeta_m}^{\beta,m}(k-1), \quad (44)$$

where

$$\alpha_{\zeta_m}^{\beta,m}(k) \triangleq \frac{\Pr \left[ \mathbf{z}(k) \mid \hat{M}_{\zeta_m}^{\beta,m}(k), Z^{k-1} \right]}{\sum_{\zeta_n} \Pr \left[ \mathbf{z}(k) \mid \hat{M}_{\zeta_n}^{\beta,m}(k), Z^{k-1} \right] \hat{\mu}_{\zeta_n}^{\beta,m}(k-1)}. \quad (45)$$

It is required for these probabilities to converge to the right ones, i.e., all converge to zero except  $\{\hat{\mu}_{n_l}^{q,l}(k)\}_{l=1}^L$  and  $\{\hat{\mu}_{o_j}^{r,j}(k)\}_{j=1}^J$  converge to one. A sufficient condition for this

convergence to happen is that there exists some  $k_0$  such that  $\forall k \geq k_0$ , the following holds

$$\operatorname{argmax}_{\zeta_m} \left[ \alpha_{\zeta_m}^{\beta, m}(k) \right] = \begin{cases} n_m, & \text{if } u \leq \sum_{l=1}^L r_l, \\ o_m, & \text{otherwise,} \end{cases} \quad (46)$$

where  $n_m$  and  $o_m$  are the indexes of the true modes of the  $m$ th process noise and measurement noise elements, respectively. The above condition is similar to

$$\operatorname{argmax}_{\zeta_m} \left\{ \Pr \left[ z(k) | \hat{M}_{\zeta_m}^{\beta, m}(k), Z^{k-1} \right] \right\} = \begin{cases} n_m, & \text{if } u \leq \sum_{l=1}^L r_l, \\ o_m, & \text{otherwise,} \end{cases} \quad (47)$$

$\forall k \geq k_0$ , since  $\sum_{\zeta_n} \Pr \left[ z(k) | \hat{M}_{\zeta_n}^{\beta, m}(k), Z^{k-1} \right] \hat{\mu}_{\zeta_n}^{\beta, m}(k-1)$  is a constant with respect to  $\zeta_m$ . The condition in (46) says that at each time step  $k \geq k_0$ , the closest constructed model to the true model is the one matched to  $n_m$ , if  $u \leq \sum_{l=1}^L r_l$  or  $o_m$  otherwise. Note that the reduced order MM estimator can be viewed as a standard MM estimator whose mode models are different than the true model. In such cases, when the assumed modes in the standard MM estimator do not contain the true mode of the system, it has been proven in [?] that the standard MM estimator will converge to the mode whose model is the closest to the true model. As such, if (46) holds, then (38)–(39) will be satisfied and the reduced-order MM estimator will converge to the matched KF. It is important to also note that the sufficient condition in (47) holds only when the process and measurement noise statistics are statics, i.e., no mode switching is happening. A summary of the reduced-order MM algorithm is given in Fig. 2.

**Remark:** Intuitively, the condition in (46) is more likely to be satisfied when the models of different modes are “different” enough. For example, assuming only 1 scalar process noise element with two possible models, then (46) is more likely to hold when  $|Q_1 - Q_2| = 10$  rather than  $|Q_1 - Q_2| = 0.01$ .

#### IV. SIMULATION RESULTS

It is important to note that the proposed reduced-order MM estimator is a different algorithm than the standard MM altogether. As such, one should not expect the same performance as the standard MM estimator. A sufficient condition for the reduced-order MM to achieve optimality was presented in Section III-D; however, this condition may not always be satisfied. In such cases, characterizing the loss in performance quickly becomes intractable and is left for future work. This paper resorts to simulations to characterize the performance of the reduced-MM estimator. To this end, the following system is considered

$$\mathbf{x}(k+1) = \begin{bmatrix} 1 & T \\ 0 & 1 \end{bmatrix} \mathbf{x}(k) + \mathbf{w}(k), \quad (48)$$

$$z(k) = [0.02 \quad 0.1] \mathbf{x}(k) + v(k), \quad (49)$$

where  $T = 0.1$  s is the sampling time;  $\mathbf{x} = [x_1, x_2]^T$  is the state vector, where  $x_1$  is expressed in meters and  $x_2$  in meters

per second;  $\mathbf{w}$  is a zero-mean white sequence with covariance  $\mathbf{Q}$  given by

$$\mathbf{Q} = \sum_{l=1}^2 \Gamma_l \mathbf{Q}^l \Gamma_l^T, \quad (50)$$

where

$$\Gamma_1 \triangleq [1 \quad 0]^T, \quad \mathbf{Q}^1 \triangleq S_1 T,$$

$$\Gamma_2 \triangleq \mathbf{I}_{2 \times 2}, \quad \mathbf{Q}^2 \triangleq \begin{bmatrix} S_2 \frac{T^3}{3} & S_2 \frac{T^2}{2} \\ S_2 \frac{T^2}{2} & S_2 T \end{bmatrix},$$

the power spectra  $S_1$  and  $S_2$  are from the sets  $\mathcal{S}_1 = \{0.1, 4, 8\}$  and  $\mathcal{S}_2 = \{0.001, 0.4, 5\}$ , respectively; and  $v(k)$  is a zero-mean white Gaussian random variable with variance  $R$  from the set  $\mathcal{R} = \{1, 8, 10\}$ . It can be clearly seen that the system defined in (48)–(49) is in the form of the one defined in (1)–(2) with two process noise elements and one measurement noise element, each of which can be in one of three modes. As such,  $3^2 \times 3^1 = 27$  filters are needed to implement a standard MM estimator, while only  $(2 \times 3) + (1 \times 3) = 9$  filters are needed for the reduced-order MM estimator. The true system model is set to be  $S_1 = 4, S_2 = 0.4$ , and  $R = 8$ . The initial state statistics are chosen as  $\mathbf{x} \sim \mathcal{N}(\mathbf{x}_0, \mathbf{P}_0)$ , where  $\mathbf{x}_0 \triangleq [2, 1]^T$  and  $\mathbf{P}_0 \triangleq \operatorname{diag}[1000, 10]$ . Then, five estimators are implemented for comparative analysis:

- i **Matched KF:** A single KF matched to the true model,
- ii **Standard MM estimator:** A standard MM estimator running all 27 filters each matched to a combination from the set  $\mathcal{S}_1 \times \mathcal{S}_2 \times \mathcal{R}$ ,
- iii **Reduced-order MM estimator:** The proposed reduced-order MM estimator with 9 filters, which is the efficient implementation of the standard MM estimator, and
- iv **Mismatched KF - min Q:** A single KF assuming  $S_1 = 0.1, S_2 = 0.001$ , and  $R = 1$ .
- v **Mismatched KF - max Q:** A single KF assuming  $S_1 = 8, S_2 = 5$ , and  $R = 10$ .

The root mean-squared error (RMSE) of each of the states  $x_1$  and  $x_2$  was computed from  $10^4$  Monte Carlo realizations for each filter and are shown in Fig. 3 along with the RMSE calculated by propagating the Riccati equation. It can be clearly seen from Fig. 3 that while the matched KF yields the lowest RMSE matching the theoretical RMSE obtained by the Riccati equation, the standard and reduced-order MM estimators achieve comparable performance. The mismatched KF with maximum  $\mathbf{Q}$  yields acceptable RMSE for  $x_1$ ; however, the RMSE for  $x_2$  is significantly large. The fraction of increase in the final RMSEs of the reduced-order MM from the standard MM estimator are 1.40% and 1.90% for  $x_1$  and  $x_2$ , respectively. This small loss in performance between the reduced-order and standard MM estimator comes at the benefit of a significant reduction in the number of filters needed, which in this case is a 300% reduction. The fraction of realizations in which the standard MM estimator converged to the wrong modes was 12.8% and 24.01% for the reduced-order MM estimator. Moreover, the fraction of realizations the reduced-order MM estimator converged to different modes than the standard estimator was computed to be 14.82%.

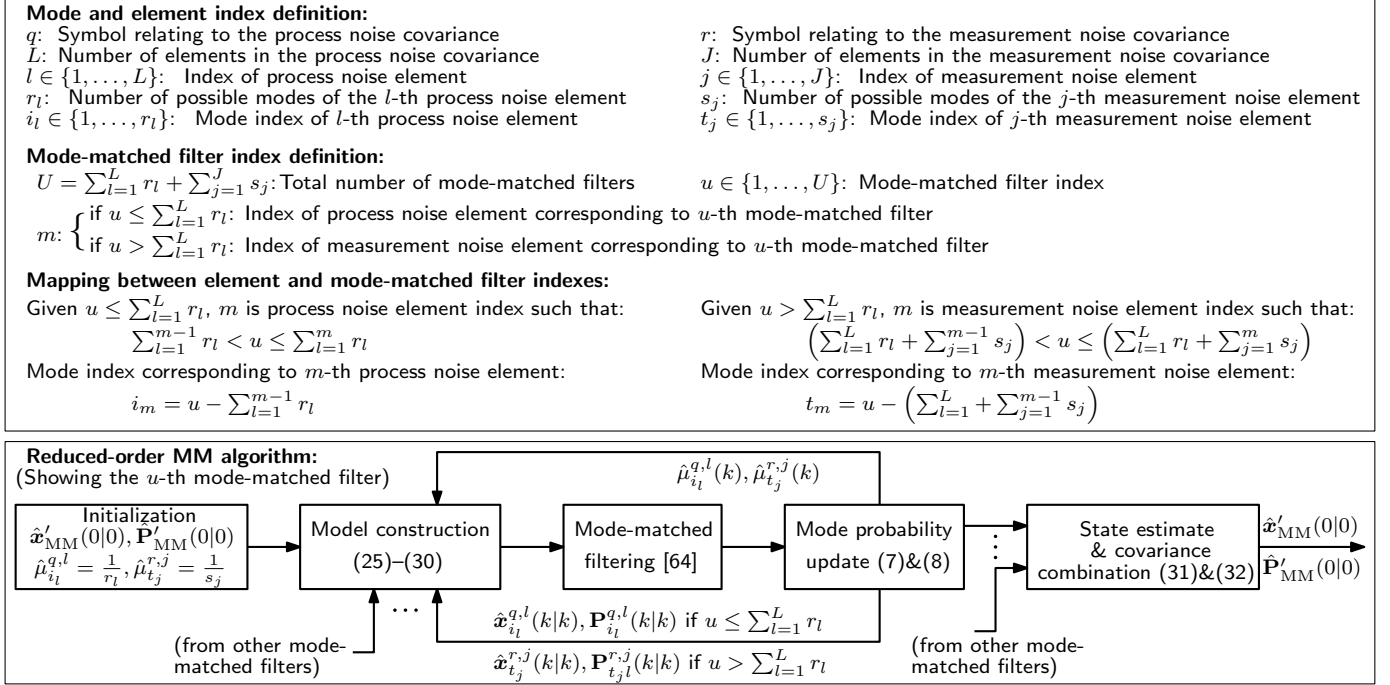


Fig. 2. Summary of the reduced-order algorithm showing how the indexes are defined and calculated as well as a block diagram of the filtering steps.

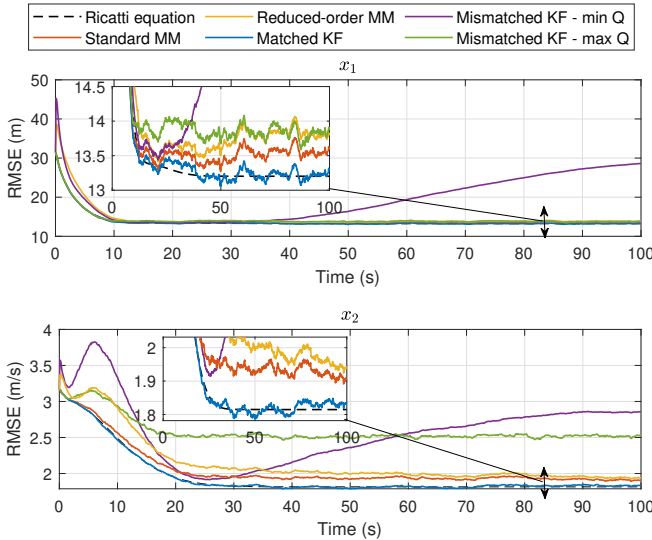


Fig. 3. Monte Carlo simulations results showing the RMSE for each error state  $x_1$  and  $x_2$  computed from  $10^4$  realizations for each of the estimators for  $\mathcal{S}_1 = \{0.1, 4, 8\}$ ,  $\mathcal{S}_2 = \{0.001, 0.4, 5\}$ , and  $\mathcal{R} = \{1, 8, 10\}$ . The RMSE was also calculated by propagating the Riccati equation and plotted for comparison.

In order to explore the case where the reduced-order MM fails to approximate the standard MM, the sets  $\mathcal{S}_1$ ,  $\mathcal{S}_2$ , and  $\mathcal{R}$  are changed to  $\mathcal{S}_1 = \{3.5, 4, 8\}$ ,  $\mathcal{S}_2 = \{0.01, 0.4, 8\}$ , and  $\mathcal{R} = \{6, 8, 10\}$ . Then, five estimators are implemented for comparative analysis:

- i **Matched KF:** A single KF matched to the true model,
- ii **Standard MM estimator:** A standard MM estimator running all 27 filters each matched to a combination from the set  $\mathcal{S}_1 \times \mathcal{S}_2 \times \mathcal{R}$ ,
- iii **Reduced-order MM estimator:** The proposed reduced-

order MM estimator with 9 filters, which is the efficient implementation of the standard MM estimator, and

- iv **Mismatched KF - min Q:** A single KF assuming  $S_1 = 3.4$ ,  $S_2 = 0.01$ , and  $R = 6$ .
- v **Mismatched KF - max Q:** A single KF assuming  $S_1 = 8$ ,  $S_2 = 0.8$ , and  $R = 10$ .

The new results are shown in Fig. 4. As can be seen from the figure, when there is less distinction between the modes, reflected by the fact that the values in  $\mathcal{S}_1$ ,  $\mathcal{S}_2$ , and  $\mathcal{R}$  are now closer to one another, the reduced-order MM struggles to properly approximate the standard MM. This is an indication that the sufficient condition discussed in Section III-D is not satisfied. Although the reduced-order MM performed worse after changing  $\mathcal{S}_1$  and  $\mathcal{S}_2$ , it still yielded acceptable performance, especially compared to the mismatched KF with the minimum  $\mathbf{Q}$ . The mismatched KF with the maximum  $\mathbf{Q}$  yields acceptable RMSEs. This second set of simulation results highlights the importance of the condition in Section III-D for both MM estimators and suggest that when the modes are “close enough”, there is not much gain in using a MM estimation approach over the maximum  $\mathbf{Q}$  filter. However, in practical MM applications, the modes will be significantly distinct. In such cases, the reduced-order MM would be desirable as it performs similarly to the standard MM estimator but with the fraction of its complexity. This is illustrated in the next section. The simulation results are summarized in Table I.

## V. CASE STUDY: UAV NAVIGATION WITH CELLULAR SIGNALS OF OPPORTUNITY

This section presents experimental results for the case of UAV navigation with signals of opportunity (SOPs) to validate the proposed method.

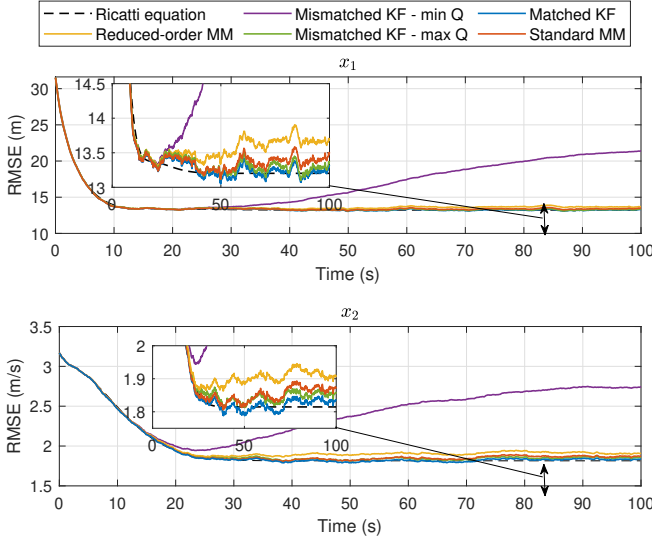


Fig. 4. Monte Carlo simulations results showing the RMSE for each error state  $x_1$  and  $x_2$  computed from  $10^4$  realizations for each of the estimators for  $\mathcal{S}_1 = \{3.5, 4, 8\}$ ,  $\mathcal{S}_2 = \{0.01, 0.4, 0.8\}$ , and  $\mathcal{R} = \{6, 8, 10\}$ . The RMSE was also calculated by propagating the Riccati equation and plotted for comparison.

TABLE I  
SUMMARY OF SIMULATION 1/SIMULATION 2 RESULTS

Estimator	Number of filters	Final RMSE for $x_1$ (m)	Final RMSE for $x_2$ (m/s)
Matched KF	1	13.32/13.32	1.835/1.835
Mismatched KF - max Q	1	13.91/13.38	2.532/1.858
Mismatched KF - min Q	1	28.63/21.39	2.861/2.744
Standard MM	27	13.79/13.51	1.893/1.874
Reduced-order MM	9	13.83/13.71	1.943/1.910

### A. System Model

In what follows, the UAV motion model, clock error models, and measurement models are described and the mode-matched EKFs are formulated.

1) *UAV Dynamics Model*: The UAV's 2-D position and velocity states,  $\mathbf{r}_r$  and  $\dot{\mathbf{r}}_r$ , respectively, are assumed to evolve according to velocity random walk dynamics. Note that it is assumed that the UAV knows its altitude from other sensors, such as a barometric altimeter. As such, the discrete-time dynamics of  $\mathbf{x}_{pv} \triangleq [\mathbf{r}_r^T, \dot{\mathbf{r}}_r^T]^T$  will be given by

$$\mathbf{x}_{pv}(k+1) = \mathbf{F}_{pv}\mathbf{x}_{pv}(k) + \mathbf{w}_{pv}(k), \quad k = 0, 1, \dots, \quad (51)$$

where  $\mathbf{w}_{pv}$  is a zero-mean, white sequence with covariance  $\mathbf{Q}_{pv}$ , and

$$\mathbf{F}_{pv} \triangleq \begin{bmatrix} \mathbf{I}_{2 \times 2} & T\mathbf{I}_{2 \times 2} \\ \mathbf{0}_{2 \times 2} & \mathbf{I}_{2 \times 2} \end{bmatrix}, \quad \mathbf{Q}_{pv} \triangleq \begin{bmatrix} \frac{T^3}{3}\tilde{\mathbf{S}}_{pv} & \frac{T^2}{2}\tilde{\mathbf{S}}_{pv} \\ \frac{T^2}{2}\tilde{\mathbf{S}}_{pv} & T\tilde{\mathbf{S}}_{pv} \end{bmatrix},$$

where  $T$  is the sampling interval,  $\tilde{\mathbf{S}}_{pv} \triangleq \text{diag}[\tilde{q}_x, \tilde{q}_y]$ , and  $\tilde{q}_x$  and  $\tilde{q}_y$  are the  $x$  and  $y$  acceleration noise power spectra, respectively.

2) *Clock Error Dynamics Model*: Let  $\mathbf{x}_{clk_n} \triangleq c[\delta t_n, \dot{\delta t}_n]^T$  denote the clock error state of the  $n$ -th

BTS, where  $\delta t_n$  is the difference between the BTS's and receiver's clock biases,  $\dot{\delta t}_n$  is the difference of their drifts, and  $c$  is the speed of light. A double integrator driven by process noise is used to model each of the clock error states. As such,  $\mathbf{x}_{clk_n}$  will evolve according to

$$\mathbf{x}_{clk_n}(k+1) = \mathbf{F}_{clk}\mathbf{x}_{clk_n}(k) + \mathbf{w}_{clk_n}(k), \quad (52)$$

where  $\mathbf{w}_{clk_n}$  is a zero-mean, white sequence with covariance  $\mathbf{Q}_{clk_n} \triangleq \mathbf{Q}_{clk_r} + \mathbf{Q}_{clk_{s_n}}$ , and

$$\mathbf{F}_{clk} \triangleq \begin{bmatrix} 1 & T \\ 0 & 1 \end{bmatrix}, \quad \mathbf{Q}_{clk_i} \triangleq \begin{bmatrix} \frac{T^3}{3}\tilde{S}_{\delta t_i} + T\tilde{S}_{\delta t_i} & \frac{T^2}{2}\tilde{S}_{\delta t_i} \\ \frac{T^2}{2}\tilde{S}_{\delta t_i} & T\tilde{S}_{\delta t_i} \end{bmatrix},$$

where  $\tilde{S}_{\delta t_i}$  and  $\tilde{S}_{\dot{\delta t}_i}$  are the clock bias and clock drift process noise power spectra, and  $i$  denotes either the receiver-mounted UAV  $r$  or the  $n$ -th BTS  $s_n$ . The power spectra  $\tilde{S}_{\delta t_i}$  and  $\tilde{S}_{\dot{\delta t}_i}$  can be related to the power-law coefficients  $\{h_\alpha\}_{\alpha=-2}^2$ , which have been shown through laboratory experiments to characterize the power spectral density of the fractional frequency deviation  $y(t)$  of an oscillator from nominal frequency, namely,  $\tilde{S}_y(f) = \sum_{\alpha=-2}^2 h_\alpha f^\alpha$  [68]. It is common to approximate such relationships by considering only the frequency random-walk coefficient  $h_{-2}$  and the white frequency coefficient  $h_0$ , which lead to  $\tilde{S}_{\delta t_i} \approx h_{0,i}$  and  $\tilde{S}_{\dot{\delta t}_i} \approx 2\pi^2 h_{-2,i}$  [66], [69]. It is important to note that the process noise in the clock error states will be correlated due to receiver's process noise; hence,

$$\mathbb{E}[\mathbf{w}_{clk_n}(k)\mathbf{w}_{clk_m}^T(k)] = \begin{cases} \mathbf{Q}_{clk_r} + \mathbf{Q}_{clk_{s_n}}, & \text{if } n = m, \\ \mathbf{Q}_{clk_r}, & \text{otherwise.} \end{cases} \quad (53)$$

3) *Measurement Model*: Carrier phase measurements are more precise than pseudorange measurements [70] and will be hence used in what follows. Note that the precision of carrier phase measurements come at the price of additional ambiguities, which have been shown lumped into the clock biases  $\delta t_n$ . The carrier phase measurement expressed in meters can be modeled as

$$z_n(k) = \|\mathbf{r}_r(k) - \mathbf{r}_{s_n}\|_2 + c\delta t_n(k) + v_n(k), \quad (54)$$

where  $\mathbf{r}_{s_n}$  is the  $n$ -th BTS's known 2-D position vector and  $v_n(k)$  is the measurement noise, which is modeled as a zero-mean, white Gaussian random variable with variance  $\sigma_n^2(k)$ . The statistics of  $v_n(k)$  are discussed in [70].

4) *EKF Model*: The EKF estimates the UAV-mounted receiver's position and velocity and the clock error states for all BTSs, namely

$$\mathbf{x}(k) \triangleq [\mathbf{x}_{pv}^T(k), \mathbf{x}_{clk_1}^T(k), \dots, \mathbf{x}_{clk_N}^T(k)]^T, \quad (55)$$

where  $N$  is the total number of available BTSs. As such, it follows that the dynamics of  $\mathbf{x}$  and the measurement model will be given by

$$\mathbf{x}(k+1) = \mathbf{F}\mathbf{x}(k) + \mathbf{w}(k) \quad (56)$$

$$\mathbf{z}(k) = \mathbf{h}[\mathbf{x}(k)] + \mathbf{v}(k), \quad (57)$$

where  $\mathbf{F} \triangleq \text{diag}[\mathbf{F}_{pv}, \mathbf{F}_{clk}, \dots, \mathbf{F}_{clk}]; \mathbf{h}[\mathbf{x}(k)] \triangleq [h_1[\mathbf{x}(k)], \dots, h_N[\mathbf{x}(k)]]^T, h_n[\mathbf{x}(k)] \triangleq \|\mathbf{r}_r(k) - \mathbf{r}_{s_n}\|_2 +$

$c\delta t_n(k)$ ,  $\mathbf{z}(k) \triangleq [z_1(k), \dots, z_N(k)]^T$ ;  $\mathbf{w}(k)$  is a discrete-time zero-mean white sequence with covariance  $\mathbf{Q} \triangleq \text{diag}[\mathbf{Q}_{\text{pv}}, \mathbf{Q}_{\text{clk}}]$ ,

$$\mathbf{Q}_{\text{clk}} \triangleq \begin{bmatrix} \mathbf{Q}_{\text{clk},r} + \mathbf{Q}_{\text{clk},1} & \mathbf{Q}_{\text{clk},r} & \dots & \mathbf{Q}_{\text{clk},r} \\ \mathbf{Q}_{\text{clk},r} & \mathbf{Q}_{\text{clk},r} + \mathbf{Q}_{\text{clk},2} & \dots & \mathbf{Q}_{\text{clk},r} \\ \vdots & \vdots & \ddots & \vdots \\ \mathbf{Q}_{\text{clk},r} & \mathbf{Q}_{\text{clk},r} & \dots & \mathbf{Q}_{\text{clk},r} + \mathbf{Q}_{\text{clk},N} \end{bmatrix};$$

and  $\mathbf{v}(k) \triangleq [v_1(k), \dots, v_N(k)]^T$  is a discrete-time zero-mean white Gaussian sequence with covariance  $\mathbf{R}(k) \triangleq \text{diag}[\sigma_1^2(k), \dots, \sigma_N^2(k)]$ . It can be readily seen that  $\mathbf{Q}$  is of the form defined in (3), particularly, it can be expressed as

$$\mathbf{Q} = \mathbf{\Gamma}_{\text{pv}} \mathbf{Q}_{\text{pv}} \mathbf{\Gamma}_{\text{pv}}^T + \mathbf{\Gamma}_r \mathbf{Q}_{\text{clk},r} \mathbf{\Gamma}_r^T + \sum_{n=1}^N \mathbf{\Gamma}_{s_n} \mathbf{Q}_{\text{clk},s_n} \mathbf{\Gamma}_{s_n}^T, \quad (58)$$

where  $\mathbf{\Gamma}_{\text{pv}} \triangleq [\mathbf{I}_{4 \times 4}, \mathbf{0}_{4 \times 2N}]^T$ ,  $\mathbf{\Gamma}_r \triangleq [\mathbf{0}_{2 \times 4}, \mathbf{I}_{2 \times 2}, \dots, \mathbf{I}_{2 \times 2}]^T$ , and  $\mathbf{\Gamma}_{s_n} \triangleq [\mathbf{0}_{2 \times 4}, \mathbf{0}_{2 \times 2}, \dots, \mathbf{0}_{2 \times 2}, \mathbf{I}_{2 \times 2}, \mathbf{0}_{2 \times 2}, \dots, \mathbf{0}_{2 \times 2}]^T$ . Each EKF is producing an estimate  $\hat{\mathbf{x}}(k|j) = \mathbb{E}[\mathbf{x}(k) | \mathbf{z}(1), \dots, \mathbf{z}(j)]$ ,  $j \leq k$ , with an associated estimation error covariance  $\mathbf{P}(k|j) = \mathbb{E}[\tilde{\mathbf{x}}(k|j)\tilde{\mathbf{x}}^T(k|j)]$ , where  $\tilde{\mathbf{x}}(k|j) \triangleq \mathbf{x}(k) - \hat{\mathbf{x}}(k|j)$  is the estimation error. The current state estimate  $\hat{\mathbf{x}}(k|k)$  and its associated estimation error covariance  $\mathbf{P}(k|k)$  are obtained using the standard EKF equations. It has been proven in [70] that the system in (56)–(57) is observable for  $N \geq 2$  and the estimation error will be bounded in a mean-squared sense. The measurement Jacobian  $\mathbf{H}(k)$  used in the EKF estimation error covariance update is given by

$$\mathbf{H}(k) = \begin{bmatrix} \mathbf{G}(k) & \mathbf{I}_{N \times N} & \mathbf{0}_{(N+2) \times (N+2)} \end{bmatrix}, \quad (59)$$

$$\mathbf{G}(k) \triangleq \begin{bmatrix} \frac{\mathbf{r}_r(k) - \mathbf{r}_{s_1}}{\|\mathbf{r}_r(k) - \mathbf{r}_{s_1}\|_2} & \dots & \frac{\mathbf{r}_r(k) - \mathbf{r}_{s_N}}{\|\mathbf{r}_r(k) - \mathbf{r}_{s_N}\|_2} \end{bmatrix}^T, \quad (60)$$

where  $\mathbf{G}(k)$  is evaluated at  $\hat{\mathbf{x}}(k|j)$ . As such, linearizing the system defined in (56)–(57) around the estimate yields

$$\tilde{\mathbf{x}}(k+1|k) = \mathbf{F}\tilde{\mathbf{x}}(k|k) + \mathbf{w}(k), \quad (61)$$

$$\boldsymbol{\nu}(k) = \mathbf{H}(k)\tilde{\mathbf{x}}(k|k-1) + \mathbf{v}(k), \quad (62)$$

where  $\boldsymbol{\nu}(k) \triangleq \mathbf{z}(k) - \mathbf{h}[\hat{\mathbf{x}}(k|k-1)]$  is the innovation vector. The system in (61)–(62) is an LTV system whose process noise covariance given in (58) is of the form in (3). Consequently, the proposed reduced-order MM estimator can be used to estimate  $\mathbf{x}$ .

### B. Hardware Setup and Filter Description

For this experiment, a DJI Matrice 600 was equipped with an Ettus E312 universal software radio peripheral (USRP), a consumer-grade 800/1900 MHz cellular antenna, and a small consumer-grade GPS antenna to discipline the on-board oscillator. The UAV-mounted receiver was tuned to listen to cellular signals in the 800 MHz band allocated for cellular communication in the U.S. Specifically, the E312 USRP was tuned to a 882.75 MHz carrier frequency, which is a cellular CDMA channel allocated for the U.S. cellular

provider Verizon Wireless. Samples of the received signals were stored for off-line post-processing. The cellular carrier phase measurements were given at a rate of 37.5 Hz, i.e.,  $T = 26.67$  ms. The ground-truth reference for the UAV trajectory was taken from its on-board navigation system, which uses GPS, an inertial measurement unit (IMU), and other sensors. The hovering horizontal precision of the UAV is reported to be 1.5 meters by DJI. The  $x$  and  $y$  continuous-time acceleration noise spectra were set to  $\tilde{q}_x = \tilde{q}_y = 0.03$  m<sup>2</sup>/s<sup>3</sup>. Throughout the experiment, the receiver on-board the UAV was listening to 7 cellular CDMA BTSs whose positions were determined beforehand. The experimental setup and BTS layout is shown in Fig. 5.

In this experiment, the statistics of the process noise driving the receiver and BTS clocks are unknown. The qualities of the BTS clock oscillators are assumed to range between that of a typical oven-controlled crystal oscillator (OCXO) and that of a high-quality OCXO. The quality of the receiver clock oscillator is assumed to range between that of a typical temperature compensated crystal oscillator (TCXO) and that of a typical OCXO. As such, each clock error state is assumed to be in one of two modes. The  $h_0$  and  $h_{-2}$  parameters of the aforementioned oscillators are given in Table II. Three estimators of  $\mathbf{x}$  are implemented for a comparative study:

- i **Standard EKF:** A single EKF matched to a typical TCXO for the receiver clock and typical OCXOs for the BTSs' clocks,
- ii **Standard MM estimator:** A standard MM estimator running  $2^8 = 256$  filters each matched to a combination of typical TCXO or OCXO for the receiver clock and typical or high-quality OCXO for the BTSs' clocks, and
- iii **Reduced-order MM estimator:** The proposed reduced-order MM estimator with  $2 \times 8 = 16$  filters, which is the efficient implementation of the standard MM estimator.

Each EKF was initialized according to the framework in [70] with initial position estimates obtained from the UAVs' on-board navigation systems and with equal mode probabilities. I.

TABLE II  
OSCILLATOR PARAMETERS

Parameter	Value
High-quality OCXO $\{h_0, h_{-2}\}$	$\{2.6 \times 10^{-22}, 4.0 \times 10^{-26}\}$
Typical OCXO $\{h_0, h_{-2}\}$	$\{8.0 \times 10^{-20}, 4.0 \times 10^{-23}\}$
Typical TCXO $\{h_0, h_{-2}\}$	$\{9.4 \times 10^{-20}, 3.8 \times 10^{-21}\}$

### C. Experimental Results and Discussion

The UAV's total traversed trajectory was 3.02 km, which was completed in 320 seconds. The true and estimated UAV trajectories are shown in Fig. 6. The total position RMSE was calculated for each estimator is tabulated in Table III along with the final estimation errors.

It can be seen from Fig. 6 and Table III that both MM estimators perform significantly better than the standard EKF. The time history of the mode probabilities for the standard MM and reduced-order MM estimators shown in Fig. 7 shed

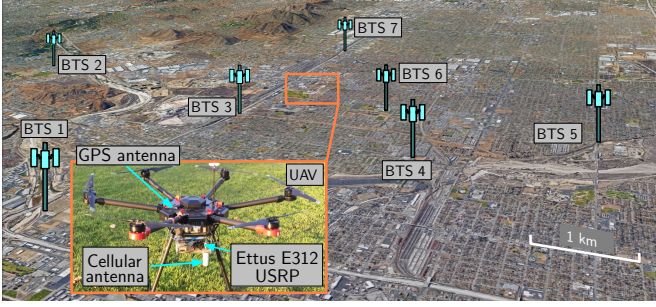


Fig. 5. Experimental setup and BTS layout. The environment consists of 7 cellular CDMA BTSs.

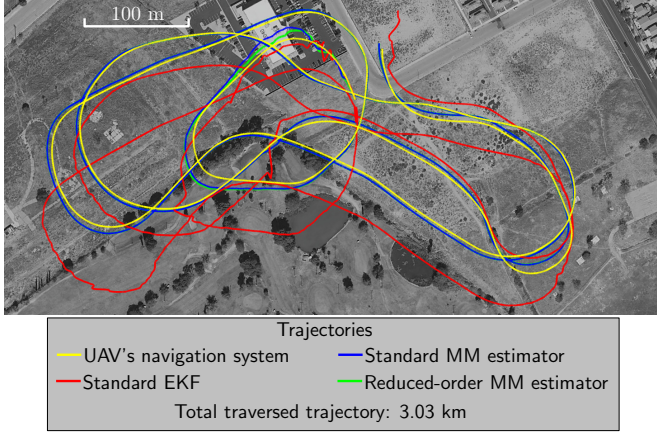


Fig. 6. True UAV trajectory and estimated UAV trajectories via the three estimators. Map data: Google Earth.

light on why both MM estimators performed significantly better than the standard EKF. It can be seen from Fig. 7 that all mode probabilities in the standard MM estimator converged to zero, except for that of mode 129, which corresponds to the receiver clock being a typical TCXO and all BTSs' clocks being high-quality OCXOs. Convergence happened within the first 5 seconds of the experiment. That is, throughout the remaining 315 seconds, the standard MM behaved as a single EKF matched to mode 129. In contrast, the standard EKF considered in this experiment was matched to a receiver clock being a typical TCXO while the BTS clocks were assumed to be typical OCXOs. The model assumed by the standard EKF apparently mismatches the true model, resulting in large EKF errors. Such large errors were mitigated by the standard MM which converged to mode 129, indicating that the true model is closer to the one of mode 129 than the one assumed by the standard EKF. What is more interesting is that the reduced-order MM estimator mode probabilities converged to the same values as the standard MM. That is, the probability of the receiver clock being a typical TCXO converged to 1 and the probability of all BTSs' clocks being OCXOs converged to 1 as well. In other words, the reduced-order MM also behaved as a single EKF matched to mode 129 after convergence. Consequently, one should expect that after some transient, the reduced-order MM estimator should converge to the standard MM estimator. This can be seen in Fig. 6, where the green curve (from the reduced-order MM estimator) converges to blue one (from the standard MM estimator) after

TABLE III  
POSITION RMSES AND FINAL ERRORS

Estimator	Number of filters	RMSE	Final error
Standard EKF	1	38.76 m	40.03 m
Standard MM	256	5.73 m	6.21 m
Reduced-order MM	16	5.67 m	6.25 m

some transient. This is also reflected in the RMSE and final error values in Table III. To see this even more, the EKF position errors and the associated  $\pm 3\sigma$  bounds are shown in Fig. 8 for each estimator. A closer look at the EKF errors and  $\pm 3\sigma$  bounds of both MM estimators shows small differences in the first few seconds and almost identical behavior afterwards.

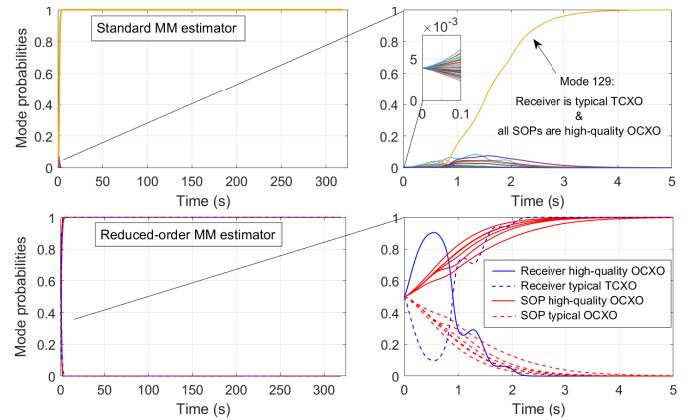


Fig. 7. Time history of the probabilities of the standard and reduced-order MM estimators.

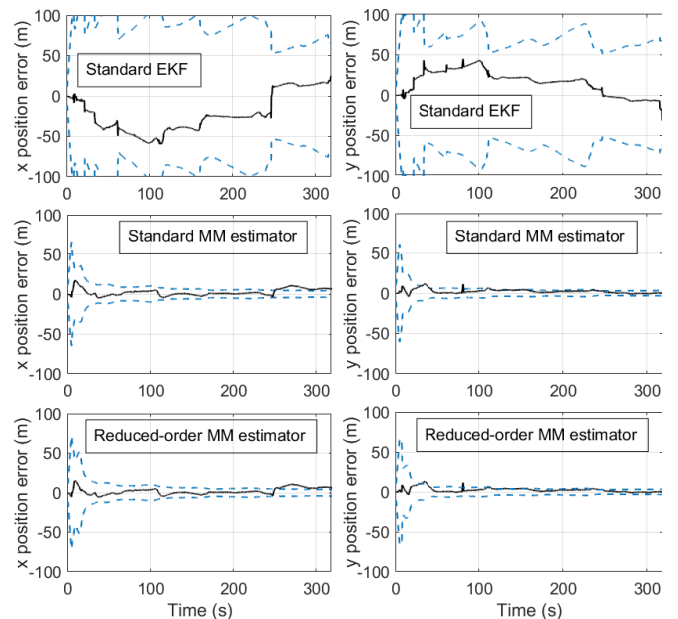


Fig. 8. UAV's position estimation error trajectories (solid black lines) and associated  $\pm 3\sigma$  bounds (dashed blue lines) for each estimator.

## VI. CONCLUSION

A reduced-order MM estimator for static noise identification in dynamic stochastic systems was proposed. The proposed algorithm reduces the computational complexity of MM estimation from exponential to polynomial by constructing a significantly smaller set of mode models which are updated every time step. It is assumed that the constructed mode models do not change significantly between time steps, which can be guaranteed by the smoothness of the mode probabilities. It is shown that the reduced-order MM estimator converges to the standard MM estimator when the mode models are sufficiently distinct. Two sets of Monte Carlo simulations were conducted: (i) one where the mode models were significantly distinct and (ii) one where mode models were very close. In the first set of simulations, the reduced-order MM estimator performs nearly similar to the standard MM estimator while some degradation is observed in the second set. However, the reduced-order MM yielded acceptable performance in both simulation sets and was implemented with a fraction of the standard MM estimator's complexity. Experimental results of opportunistic navigation on a UAV in the case of unknown transmitter clock process noise covariances were also presented to further validate the proposed approach. The experimental results show a UAV navigating for more than 5 minutes over a trajectory of more than 3 km, with a final position error of 6.21 m obtained using the standard MM estimator versus a final position error of 6.25 m obtained using the proposed reduced-order MM estimator. A standard extended Kalman filter (EKF) was implemented for comparative analysis, showing a final error of 40.03 m. In the experiments, the reduced-order MM estimator was implemented with 16 filters, while the standard MM was implemented with 256 filters. While the proposed approach is showing promising results when the mode models are significantly distinct, a necessary condition for optimality is needed and is left as future work.

## ACKNOWLEDGMENT

The authors would like to thank Joshua Morales and Kimia Shamaei for their help with data collection.

 APPENDIX  
 PROOF OF LEMMA III.1

This appendix provides the proof of Lemma III.1.

*Proof.* Note the marginalization

$$\begin{aligned} & \sum_{t_1} \dots \sum_{t_J} \mu_{i_1, \dots, i_L, t_1, \dots, t_J}(k) \\ &= \sum_{t_1} \dots \sum_{t_J} \Pr [M_{i_1}^1, \dots, M_{i_L}^L, N_{t_1}^1, \dots, N_{t_J}^J | Z^k] \\ &= \Pr [M_{i_1}^1, \dots, M_{i_L}^L | Z^k] \\ &\triangleq \mu_{i_1, \dots, i_L}^q(k). \end{aligned} \quad (63)$$

Using (63), (20) becomes

$$\begin{aligned} \hat{\mathbf{Q}}(k) &= \sum_{i_1} \dots \sum_{i_L} \mu_{i_1, \dots, i_L}^q(k) \mathbf{\Gamma}_1 \mathbf{Q}_{i_1}^1 \mathbf{\Gamma}_1^\top + \dots \\ &+ \sum_{i_1} \dots \sum_{i_L} \mu_{i_1, \dots, i_L}^q(k) \mathbf{\Gamma}_L \mathbf{Q}_{i_L}^L \mathbf{\Gamma}_L^\top \end{aligned}$$

$$\begin{aligned} &= \sum_{i_1} \mathbf{\Gamma}_1 \mathbf{Q}_{i_1}^1 \mathbf{\Gamma}_1^\top \sum_{i_2} \dots \sum_{i_L} \mu_{i_1, \dots, i_L}^q(k) + \dots \\ &+ \sum_{i_L} \mathbf{\Gamma}_L \mathbf{Q}_{i_L}^L \mathbf{\Gamma}_L^\top \sum_{i_1} \dots \sum_{i_{L-1}} \mu_{i_1, \dots, i_L}^q(k). \end{aligned} \quad (64)$$

Moreover, define the following marginal probabilities

$$\begin{aligned} & \sum_{i_1} \dots \sum_{i_{l-1}} \sum_{i_{l+1}} \dots \sum_{i_L} \mu_{i_1, \dots, i_L}^q(k) \\ &= \sum_{i_1} \dots \sum_{i_{l-1}} \sum_{i_{l+1}} \dots \sum_{i_L} \Pr [M_{i_1}^1, \dots, M_{i_L}^L | Z^k] \\ &= \Pr [M_{i_l}^l | Z^k] \\ &\triangleq \mu_{i_l}^{q,l}(k). \end{aligned} \quad (65)$$

Subsequently, the estimated process noise covariance may be expressed as

$$\begin{aligned} \hat{\mathbf{Q}}(k) &= \sum_{i_1} \mathbf{\Gamma}_1 \mathbf{Q}_{i_1}^1 \mathbf{\Gamma}_1^\top \mu_{i_1}^{q,1}(k) + \dots + \sum_{i_L} \mathbf{\Gamma}_L \mathbf{Q}_{i_L}^L \mathbf{\Gamma}_L^\top \mu_{i_L}^{q,L}(k) \\ &= \sum_{l=1}^L \sum_{i_l} \mu_{i_l}^{q,l}(k) \mathbf{\Gamma}_l \mathbf{Q}_{i_l}^l \mathbf{\Gamma}_l^\top \\ &= \frac{1}{L} \left[ \sum_{l=1}^L \sum_{i_l} \mu_{i_l}^{q,l}(k) \mathbf{\Gamma}_l \mathbf{Q}_{i_l}^l \mathbf{\Gamma}_l^\top + \dots + \sum_{l=1}^L \sum_{i_l} \mu_{i_l}^{q,l}(k) \mathbf{\Gamma}_l \mathbf{Q}_{i_l}^l \mathbf{\Gamma}_l^\top \right] \end{aligned} \quad (66)$$

Therefore,

$$\begin{aligned} \hat{\mathbf{Q}}(k) &= \frac{1}{L} \left\{ \left[ \sum_{i_1} \mu_{i_1}^{q,1}(k) \mathbf{\Gamma}_1 \mathbf{Q}_{i_1}^1 \mathbf{\Gamma}_1^\top + \sum_{l=2}^L \sum_{i_l} \mu_{i_l}^{q,l}(k) \mathbf{\Gamma}_l \mathbf{Q}_{i_l}^l \mathbf{\Gamma}_l^\top \right] \right. \\ &+ \dots \\ &\left. + \left[ \sum_{i_L} \mu_{i_L}^{q,L}(k) \mathbf{\Gamma}_L \mathbf{Q}_{i_L}^L \mathbf{\Gamma}_L^\top + \sum_{l=1}^{L-1} \sum_{i_l} \mu_{i_l}^{q,l}(k) \mathbf{\Gamma}_l \mathbf{Q}_{i_l}^l \mathbf{\Gamma}_l^\top \right] \right\}. \end{aligned} \quad (67)$$

Next, defining  $\bar{\mathbf{Q}}^m(k)$  according to (26) and noting that  $\sum_{i_l} \mu_{i_l}^{q,l}(k) = 1$ , the estimated process noise covariance becomes

$$\begin{aligned} \hat{\mathbf{Q}}(k) &= \frac{1}{L} \left[ \sum_{i_1} \mu_{i_1}^{q,1}(k) \mathbf{\Gamma}_1 \mathbf{Q}_{i_1}^1 \mathbf{\Gamma}_1^\top + \bar{\mathbf{Q}}^1(k) \right] \\ &+ \dots + \frac{1}{L} \left[ \sum_{i_L} \mu_{i_L}^{q,L}(k) \mathbf{\Gamma}_L \mathbf{Q}_{i_L}^L \mathbf{\Gamma}_L^\top + \bar{\mathbf{Q}}^L(k) \right] \\ &= \frac{1}{L} \left[ \sum_{i_1} \mu_{i_1}^{q,1}(k) \mathbf{\Gamma}_1 \mathbf{Q}_{i_1}^1 \mathbf{\Gamma}_1^\top + \bar{\mathbf{Q}}^1(k) \sum_{i_1} \mu_{i_1}^{q,1}(k) \right] + \dots \\ &+ \frac{1}{L} \left[ \sum_{i_L} \mu_{i_L}^{q,L}(k) \mathbf{\Gamma}_L \mathbf{Q}_{i_L}^L \mathbf{\Gamma}_L^\top + \bar{\mathbf{Q}}^L(k) \sum_{i_L} \mu_{i_L}^{q,L}(k) \right] \\ &= \frac{1}{L} \sum_{i_1} \mu_{i_1}^{q,1}(k) [\mathbf{\Gamma}_1 \mathbf{Q}_{i_1}^1 \mathbf{\Gamma}_1^\top + \bar{\mathbf{Q}}^1(k)] + \dots \\ &+ \frac{1}{L} \sum_{i_L} \mu_{i_L}^{q,L}(k) [\mathbf{\Gamma}_L \mathbf{Q}_{i_L}^L \mathbf{\Gamma}_L^\top + \bar{\mathbf{Q}}^L(k)]. \end{aligned} \quad (68)$$

Defining  $\bar{\mathbf{Q}}_{m}^m(k)$  according to (24) yields (22).

A similar approach is taken for  $\mathbf{R}(k)$ .  $\square$

## REFERENCES

- [1] C. Cadena, L. Carlone, H. Carrillo, Y. Latif, D. Scaramuzza, J. Neira, I. Reid, and J. Leonard, "Past, present, and future of simultaneous localization and mapping: Toward the robust-perception age," *IEEE Transactions on Robotics*, vol. 32, no. 6, pp. 1309–1332, 2016.
- [2] J. Choi and M. Maurer, "Local volumetric hybrid-map-based simultaneous localization and mapping with moving object tracking," *IEEE Transactions on Intelligent Transportation Systems*, vol. 17, no. 9, pp. 2440–2455, September 2016.
- [3] J. Morales, J. Khalife, and Z. Kassas, "Information fusion strategies for collaborative inertial radio SLAM," *IEEE Transactions on Intelligent Transportation Systems*, vol. 23, no. 8, pp. 12 935–12 952, August 2022.
- [4] Z. Kassas, M. Neinavaie, J. Khalife, N. Khairallah, J. Haidar-Ahmad, S. Kozhaya, and Z. Shadram, "Enter LEO on the GNSS stage: Navigation with Starlink satellites," *Inside GNSS Magazine*, vol. 16, no. 6, pp. 42–51, 2021.
- [5] J. Dunik, O. Straka, O. Kost, and J. Havlik, "Noise covariance matrices in state-space models: A survey and comparison of estimation methods—part i," *International Journal of Adaptive Control and Signal Processing*, vol. 31, no. 11, pp. 1505–1543, May 2017.
- [6] D. Alspach and H. Sorenson, "Nonlinear Bayesian estimation using Gaussian sum approximations," *IEEE Transactions on Automatic Control*, vol. 17, no. 4, pp. 439–448, August 1972.
- [7] D. Wiberg, T. Powell, and D. Ljungquist, "An online parameter estimator for quick convergence and time-varying linear systems," *IEEE Transactions on Automatic Control*, vol. 45, no. 10, pp. 1854–1863, October 2000.
- [8] L. Zhong and C. Shing-Chow, "Adaptive fading Bayesian unscented Kalman filter and smoother for state estimation of unmanned aircraft systems," *IEEE Access*, vol. 8, pp. 119 470–119 486, October 2020.
- [9] P. Gutman and M. Velger, "Tracking targets using adaptive Kalman filtering," *IEEE Transactions on Aerospace and Electronic Systems*, vol. 26, no. 5, pp. 691–699, September 1990.
- [10] R. Moghe, R. Zanetti, and M. Akella, "Adaptive Kalman filter for detectable linear time invariant systems," *Journal of Guidance, Control, and Dynamics*, vol. 42, no. 10, pp. 2197–2205, 2019.
- [11] N. Stacey and S. D'Amico, "Adaptive and dynamically constrained process noise estimation for orbit determination," *IEEE Transactions on Aerospace and Electronic Systems*, vol. 57, no. 5, pp. 2920–2937, October 2021.
- [12] P. Bélanger, "Estimation of noise covariance matrices for a linear time-varying stochastic process," *Automatica*, vol. 10, no. 3, pp. 267–275, 1974.
- [13] B. Odelson, M. Rajamani, and J. Rawlings, "A new autocovariance least-squares method for estimating noise covariances," *Automatica*, vol. 42, no. 2, pp. 303–308, 2006.
- [14] J. Dunik, O. Straka, and M. Simandl, "On autocovariance least-squares method for noise covariance matrices estimation," *IEEE Transactions on Automatic Control*, vol. 62, no. 2, pp. 967–972, February 2017.
- [15] R. Kashyap, "Maximum likelihood identification of stochastic linear systems," *IEEE Transactions on Automatic Control*, vol. 15, no. 1, pp. 25–34, February 1970.
- [16] R. Shumway and D. Stoffer, "An approach to time series smoothing and forecasting using the EM algorithm," *Journal of Time Series Analysis*, vol. 3, no. 4, pp. 253–264, July 1982.
- [17] V. Bavdekar, A. Deshpande, and S. Patwardhan, "Identification of process and measurement noise covariance for state and parameter estimation using extended Kalman filter," *Journal of Process Control*, vol. 21, no. 4, pp. 585–601, 2011.
- [18] R. Mehra, "Approaches to adaptive filtering," *IEEE Transactions on Automatic Control*, vol. 17, no. 5, pp. 693–698, October 1972.
- [19] S. Sarkka and A. Nummenmaa, "Recursive noise adaptive Kalman filtering by variational Bayesian approximations," *IEEE Transactions on Automatic Control*, vol. 3, no. 4, pp. 596–600, March 2009.
- [20] Y. Yang and W. Gao, "A Bayesian solution to the problem of state estimation in an unknown noise environments," *Journal of Geodesy*, vol. 80, no. 4, pp. 177–183, 2006.
- [21] C. Karlgaard, "Robust adaptive estimation for autonomous rendezvous in elliptical orbit," Ph.D. dissertation, Virginia Polytechnic Institute State University, Blacksburg, VA USA, 2019.
- [22] B. Friedland, "Estimating noise variances by using multiple observers," *IEEE Transactions on Aerospace and Electronic Systems*, vol. 18, no. 4, pp. 442–448, July 1982.
- [23] R. Reynolds, "Robust estimation of covariance matrices," *IEEE Transactions on Automatic Control*, vol. 35, no. 9, pp. 1047–1051, September 1990.
- [24] J. Dunik, O. Kost, O. Straka, and E. Blasch, "State and measurement noise in positioning and tracking: Covariance matrices estimation and Gaussianity assessment," in *Proceedings of IEEE/ION Position, Location, and Navigation Symposium*, April 2018, pp. 1326–1335.
- [25] Y. Bar-Shalom, "Optimal simultaneous state estimation and parameter identification in linear discrete-time systems," *IEEE Transactions on Automatic Control*, vol. 17, no. 3, pp. 308–319, 1972.
- [26] J. Burg, D. Luenberger, and D. Wenger, "Estimation of structured covariance matrices," *Proceedings of the IEEE*, vol. 70, no. 9, pp. 963–974, September 1982.
- [27] X. Li and Y. Bar-Shalom, "Multiple-model estimation with variable structure," *IEEE Transactions on Automatic Control*, vol. 41, no. 4, pp. 478–493, August 1996.
- [28] P. Hanlon and P. Maybeck, "Multiple-model adaptive estimation using a residual correlation Kalman filter bank," *IEEE Transactions on Aerospace and Electronic Systems*, vol. 36, no. 2, pp. 393–406, April 2000.
- [29] H. Blom and Y. Bar-Shalom, "The interacting multiple model algorithm for systems with Markovian switching coefficients," *IEEE Transactions on Automatic Control*, vol. 33, no. 8, pp. 780–783, August 1988.
- [30] F. Li, H. Liu, and R. Vaccaro, "Performance analysis for DOA estimation algorithms: unification, simplification, and observations," *IEEE Transactions on Aerospace and Electronic Systems*, vol. 29, no. 4, pp. 1170–1184, October 1993.
- [31] W. Ouyang, Y. Wu, and H. Chen, "INS/Odometer land navigation by accurate measurement modeling and multiple-model adaptive estimation," *IEEE Transactions on Aerospace and Electronic Systems*, vol. 57, no. 1, pp. 245–262, 2021.
- [32] M. Gomaa, O. De Silva, G. Mann, and G. Gosine, "Observability-constrained VINS for MAVs using interacting multiple model algorithm," *IEEE Transactions on Aerospace and Electronic Systems*, vol. 57, no. 3, pp. 1423–1442, June 2021.
- [33] L. Xu, X. Li, and Z. Duan, "Hybrid grid multiple-model estimation with application to maneuvering target tracking," *IEEE Transactions on Aerospace and Electronic Systems*, vol. 52, no. 1, pp. 122–136, 2016.
- [34] R. Visina, Y. Bar-Shalom, and P. Willett, "Multiple-model estimators for tracking sharply maneuvering ground targets," *IEEE Transactions on Aerospace and Electronic Systems*, vol. 54, no. 3, pp. 1404–1414, June 2018.
- [35] X. Li and Y. Bar-Shalom, "Design of an interacting multiple model algorithm for air traffic control tracking," *IEEE Transactions on Control Systems Technology*, vol. 1, no. 3, pp. 186–194, 1993.
- [36] Z. Kowalczyk and M. Sankowski, "Soft- and hard-decision multiple-model estimators for air traffic control," *IEEE Transactions on Aerospace and Electronic Systems*, vol. 46, no. 4, pp. 2056–2065, October 2010.
- [37] S. Kim, J. Choi, and Y. Kim, "Fault detection and diagnosis of aircraft actuators using fuzzy-tuning IMM filter," *IEEE Transactions on Aerospace and Electronic Systems*, vol. 44, no. 3, pp. 940–952, July 2008.
- [38] N. Sadeghzadeh-Nokhodberiz and J. Poshtan, "Distributed interacting multiple filters for fault diagnosis of navigation sensors in a robotic system," *IEEE Transactions on Systems, Man, and Cybernetics: Systems*, vol. 47, no. 7, pp. 1383–1393, July 2017.
- [39] M. Mabrouk, G. Ferre, E. Grivel, and N. Deltimple, "Interacting multiple model based detector to compensate power amplifier distortions in cognitive radio," *IEEE Transactions on Communications*, vol. 63, no. 5, pp. 1580–1593, May 2015.
- [40] X. Feng, Y. Zhao, Z. Zhao, and Z. Zhou, "Cognitive tracking waveform design based on multiple model interaction and measurement information fusion," *IEEE Access*, vol. 6, pp. 30 680–30 690, 2018.
- [41] R. Li, X., and Y. Bar-Shalom, "A recursive multiple model approach to noise identification," *IEEE Transactions on Aerospace and Electronic Systems*, vol. 30, no. 3, pp. 671–684, July 1994.
- [42] J. Raquet *et al.*, "Position, navigation, and timing technologies in the 21st century," J. Morton, F. van Diggelen, J. Spilker, Jr., and B. Parkinson, Eds. Wiley-IEEE, 2021, vol. 2, Part D: Position, Navigation, and Timing Using Radio Signals-of-Opportunity, ch. 35–43, pp. 1115–1412, doi: 10.1002/9781119458555.ch35.
- [43] Z. Kassas, J. Khalife, A. Abdallah, and C. Lee, "I am not afraid of the GPS jammer: resilient navigation via signals of opportunity in GPS-denied environments," *IEEE Aerospace and Electronic Systems Magazine*, vol. 37, no. 7, pp. 4–19, July 2022, doi: 10.1109/MAES.2022.3154110.
- [44] N. Souli, P. Kolios, and G. Ellinas, "Online relative positioning of autonomous vehicles using signals of opportunity," *IEEE Transactions on Intelligent Vehicles*, pp. 1–1, 2021, doi: 10.1109/TIV.2021.3124727.

- [45] J. McEllroy, "Navigation using signals of opportunity in the AM transmission band," Master's thesis, Air Force Institute of Technology, Wright-Patterson Air Force Base, Ohio, USA, 2006.
- [46] X. Chen, Q. Wei, F. Wang, Z. Jun, S. Wu, and A. Men, "Super-resolution time of arrival estimation for a symbiotic FM radio data system," *IEEE Transactions on Broadcasting*, vol. 66, no. 4, pp. 847–856, December 2020, doi: 10.1109/TBC.2019.2957666.
- [47] J. Honda and T. Otsuyama, "Feasibility study on aircraft positioning by using ISDB-T signal delay," *IEEE Antennas and Wireless Propagation Letters*, vol. 15, pp. 1787–1790, 2016.
- [48] C. Yang and A. Soloviev, "Mobile positioning with signals of opportunity in urban and urban canyon environments," in *Proceedings of IEEE/ION Position, Location, and Navigation Symposium*, April 2020, pp. 1043–1059, doi: 10.1109/PLANS46316.2020.9109876.
- [49] J. del Peral-Rosado, J. López-Salcedo, F. Zanier, and G. Seco-Granados, "Position accuracy of joint time-delay and channel estimators in LTE networks," *IEEE Access*, vol. 6, pp. 25 185–25 199, 2018.
- [50] J. Gante, L. Sousa, and G. Falcao, "Dethroning GPS: Low-power accurate 5G positioning systems using machine learning," *IEEE Journal on Emerging and Selected Topics in Circuits and Systems*, vol. 10, no. 2, pp. 240–252, June 2020.
- [51] J. Khalife and Z. Kassas, "On the achievability of submeter-accurate UAV navigation with cellular signals exploiting loose network synchronization," *IEEE Transactions on Aerospace and Electronic Systems*, vol. 58, no. 5, pp. 4261–4278, October 2022, doi: 10.1109/TAES.2022.3162770.
- [52] C. Yang, M. Arizabaleta-Diez, P. Weitkemper, and T. Pany, "An experimental analysis of cyclic and reference signals of 4G LTE for TOA estimation and positioning in mobile fading environments," *IEEE Aerospace and Electronic Systems Magazine*, vol. 37, no. 9, pp. 16–41, 2022, doi: 10.1109/MAES.2022.3186650.
- [53] Z. Kassas, J. Morales, and J. Khalife, "New-age satellite-based navigation – STAN: simultaneous tracking and navigation with LEO satellite signals," *Inside GNSS Magazine*, vol. 14, no. 4, pp. 56–65, 2019.
- [54] J. Khalife, M. Neinaivaie, and Z. Kassas, "The first carrier phase tracking and positioning results with Starlink LEO satellite signals," *IEEE Transactions on Aerospace and Electronic Systems*, vol. 56, no. 2, pp. 1487–1491, April 2022.
- [55] N. Jardak and Q. Jault, "The potential of LEO satellite-based opportunistic navigation for high dynamic applications," *Sensors*, vol. 22, no. 7, pp. 2541–2565, 2022.
- [56] C. Huang, H. Qin, C. Zhao, and H. Liang, "Phase - time method: Accurate Doppler measurement for Iridium NEXT signals," *IEEE Transactions on Aerospace and Electronic Systems*, vol. 58, no. 6, pp. 5954–5962, 2022.
- [57] K. Shamaei and Z. Kassas, "LTE receiver design and multipath analysis for navigation in urban environments," *NAVIGATION, Journal of the Institute of Navigation*, vol. 65, no. 4, pp. 655–675, December 2018.
- [58] K. Shamaei and Z. Kassas, "Receiver design and time of arrival estimation for opportunistic localization with 5G signals," *IEEE Transactions on Wireless Communications*, vol. 20, no. 7, pp. 4716–4731, 2021, doi: 10.1109/TWC.2021.3061985.
- [59] P. Wang and Y. Morton, "Multipath estimating delay lock loop for LTE signal TOA estimation in indoor and urban environments," *IEEE Transactions on Wireless Communications*, vol. 19, no. 8, pp. 5518–5530, 2020.
- [60] H. Dun, C. Tiberius, and G. Janssen, "Positioning in a multipath channel using OFDM signals with carrier phase tracking," *IEEE Access*, vol. 8, pp. 13 011–13 028, 2020.
- [61] T. Kazaz, G. Janssen, J. Romme, and A. Van der Veen, "Delay estimation for ranging and localization using multiband channel state information," *IEEE Transactions on Wireless Communications*, vol. 21, no. 4, pp. 2591–2607, April 2022.
- [62] Z. Kassas, V. Ghadiok, and T. Humphreys, "Adaptive estimation of signals of opportunity," in *Proceedings of ION GNSS Conference*, September 2014, pp. 1679–1689.
- [63] Z. Kassas, A. Abdallah, J. Khalife, C. Lee, J. Jurado, J. Duede, Z. Hoeffner, T. Hulsey, R. Quirarte, S. Wachtel, and R. Tay, "Received power characterization of terrestrial cellular signals on high altitude aircraft," in *Proceedings of IEEE Aerospace Conference*, March 2022, pp. 1–8, doi: 10.1109/AERO53065.2022.9843492.
- [64] R. Cassel, D. Scherer, D. Wilburne, J. Hirschauer, and J. Burke, "Impact of improved oscillator stability on LEO-based satellite navigation," in *Proceedings of ION International Technical Meeting*, January 2022, pp. 893–905.
- [65] N. Khairallah and Z. Kassas, "An interacting multiple model estimator of LEO satellite clocks for improved positioning," in *Proceedings of IEEE Vehicular Technology Conference*, 2022, pp. 1–5.
- [66] Y. Bar-Shalom, X. Li, and T. Kirubarajan, *Estimation with Applications to Tracking and Navigation*. New York, NY: John Wiley & Sons, 2002.
- [67] R. Li, X., and Y. Bar-Shalom, "A recursive multiple model approach to noise identification," *IEEE Transactions on Aerospace and Electronic Systems*, vol. 30, no. 3, pp. 671–684, July 1994.
- [68] A. Thompson, J. Moran, and G. Swenson, *Interferometry and Synthesis in Radio Astronomy*, 2nd ed. John Wiley & Sons, 2001.
- [69] R. Brown and P. Hwang, *Introduction to Random Signals and Applied Kalman Filtering with Matlab Exercises*, 4th ed. John Wiley & Sons, 2012.
- [70] J. Khalife and Z. Kassas, "Opportunistic UAV navigation with carrier phase measurements from asynchronous cellular signals," *IEEE Transactions on Aerospace and Electronic Systems*, vol. 56, no. 4, pp. 3285–3301, August 2020, doi: 10.1109/TAES.2019.2948452.



**Joe Khalife** (S'15-M'20) was a postdoctoral fellow at the University of California, Irvine and member of the Autonomous Systems Perception, Intelligence, and Navigation (ASPIN) Laboratory. He received a B.E. in Electrical Engineering, an M.S. in Computer Engineering from the Lebanese American University (LAU) and a Ph.D. in Electrical Engineering and Computer Science from the University of California, Irvine. From 2012 to 2015, he was a research assistant at LAU, and has been a member of the ASPIN Laboratory since 2015. He is a recipient of the 2016 IEEE/ION Position, Location, and Navigation Symposium (PLANS) Best Student Paper Award, 2018 IEEE Walter Fried Award, and 2021 IEEE AESS Robert T. Hill Best Dissertation Award. His research interests include opportunistic navigation, autonomous vehicles, and software-defined radio.



**Zaher (Zak) M. Kassas** (S'98-M'08-SM'11) received the B.E. degree in electrical engineering from the Lebanese American University, Beirut, Lebanon, the M.S. degree in electrical and computer engineering from The Ohio State University, Columbus, OH, USA, the M.S.E. degree in aerospace engineering and the Ph.D. in electrical and computer engineering from The University of Texas at Austin, Austin, TX, USA. He is currently a Professor of electrical and computer engineering at The Ohio State University and Director of the Autonomous Systems Perception, Intelligence, and Navigation (ASPIN) Laboratory. He is also the Director of the U.S. Department of Transportation Center: CARMEN (Center for Automated Vehicle Research with Multimodal AssurEd Navigation), focusing on navigation resiliency and security of highly automated transportation systems. His research interests include cyber-physical systems, estimation theory, navigation systems, autonomous vehicles, and intelligent transportation systems. He was the recipient of the 2018 National Science Foundation (NSF) CAREER Award, 2019 Office of Naval Research (ONR) Young Investigator Program (YIP) Award, 2022 Air Force Office of Scientific Research (AFOSR) YIP Award, 2018 IEEE Walter Fried Award, 2018 Institute of Navigation (ION) Samuel Burka Award, and 2019 ION Col. Thomas Thurlow Award. He is a Senior Editor of the IEEE TRANSACTIONS ON INTELLIGENT VEHICLES and an Associate Editor for the IEEE TRANSACTIONS ON AEROSPACE AND ELECTRONIC SYSTEMS and IEEE TRANSACTIONS ON INTELLIGENT TRANSPORTATION SYSTEMS.